

Department of Physics and Astronomy
University of Heidelberg

Bachelor Thesis in Physics
submitted by

Patrick Hanus

born in Ludwigshafen am Rhein (Germany)

26.02.2018

Entropy in Pb-Pb Collisions at the LHC

This Bachelor Thesis has been carried out by Patrick Hanus at the
Physikalisches Institut Heidelberg
under the supervision of
Prof. Klaus Reygers

Abstract. In this bachelor thesis two different methods to estimate the entropy rapidity density of lead-lead collisions with a centre-of-mass energy of $\sqrt{s_{NN}} = 2.76$ TeV at the Large Hadron Collider are investigated. The first method was introduced in *Entropy Production at RHIC* [1] by Subrata Pal and Scott Pratt and estimates the entropy rapidity density from the measured particle spectra and HBT radii of different particle species. The second method calculates the entropy rapidity density from the charged particle multiplicity using a relativistic hadron resonance gas model. The final results for the entropy rapidity density are: $dS/dy = 12272 \pm 868$ (7%) (first method) and $dS/dy = 13243 \pm 984$ (7%) (second method). Using the result of the first method, an initial temperature of $T_0 = 349$ MeV = $2.24 T_c$ at $\tau_0 = 1$ fm/c is estimated and it is concluded, that in lead-lead collisions at $\sqrt{s_{NN}} = 2.76$ TeV at the Large Hadron Collider, the Quark-Gluon Plasma is produced.

Abstract. In dieser Bachelorarbeit werden zwei verschiedene Methoden verwendet, um die Entropiedichte von Blei-Blei-Kollisionen mit einer Energie von $\sqrt{s_{NN}} = 2.76$ TeV am Large Hadron Collider zu bestimmen. Die erste Methode wurde von Subrata Pal und Scott Pratt in ihrem Paper *Entropy Production at RHIC* [1] eingeführt und schätzt die Entropiedichte anhand der gemessenen Teilchenspektren und HBT-Radien verschiedener Teilchensorten ab. Die zweite Methode berechnet die Entropiedichte mithilfe der gemessenen Teilchenmultiplizität unter Verwendung eines relativistischen Hadrongasmodells. Die Endergebnisse für die Entropiedichte sind: $dS/dy = 12272 \pm 868$ (7%) (erste Methode) bzw. $dS/dy = 13243 \pm 984$ (7%) (zweite Methode). Anhand des Ergebnisses der ersten Methode wird die Anfangstemperatur zum Zeitpunkt $\tau_0 = 1$ fm/c auf $T_0 = 349$ MeV = $2.24 T_c$ geschätzt und daraus gefolgert, dass das Quark-Gluon-Plasma in Blei-Blei-Kollisionen mit einer Energie von $\sqrt{s_{NN}} = 2.76$ TeV am Large Hadron Collider produziert wird.

Contents

1	Introduction	5
1.1	Theoretical Background	5
1.2	Motivation	10
1.3	Methods for entropy estimation	10
1.3.1	Entropy from Bjorken flow	10
1.3.2	Entropy from phase space density	12
1.3.3	Entropy from immediate equilibration	13
1.3.4	Entropy from hadron resonance gas model	13
1.3.5	Entropy from thermal model	14
1.3.6	Entropy from interacting hadron gas model	14
2	Entropy estimation according to Pal and Pratt	15
3	Entropy estimation from Relativistic Hadron Resonance Gas model	25
4	Summary	32
4.1	Pal and Pratt method	32
4.2	Relativistic Hadron Resonance Gas model	32
4.3	Overview and Synthesis of methods for entropy estimation	33
4.4	Interpretation	34

1 Introduction

Estimates of the entropy S are often needed in heavy-ion physics to evaluate different physical quantities using thermodynamic models. The problem is that the entropy is not measured directly in the experiment and instead has to be derived from the measurements of the number of charged particles N_{charged} . To do that, one needs to find a physical quantity that relates the number of charged particles to the entropy. This is not a trivial task, as one finds many different methods as well as results for entropy estimation in scientific literature. In my thesis, I will give a brief overview of selected methods and their results and then apply the method Subrata Pal and Scott Pratt used in their paper *Entropy Production at RHIC* [1] to the Large Hadron Collider (LHC) data as well as relate the entropy to the charged particle multiplicity using a relativistic hadron resonance gas model.

1.1 Theoretical Background

In the field of heavy-ion physics, we investigate what happens to matter at high temperatures and densities. In collisions of heavy nuclei at ultrarelativistic speeds, quantum chromodynamics (QCD), the theory of strong interaction between quarks and gluons, can be studied in the non-perturbative regime. At absolute zero, i.e. a temperature of 0 K, most matter we know is solid, and when heated, at some point, a phase transition to the liquid phase and after that, to the gas phase occurs. A further increase in temperature leads to the plasma phase, then to the hadron gas (HG) phase and finally to a phase of deconfined quarks and gluons, called Quark-Gluon Plasma (QGP). Heavy-ion physics aims to characterize the QGP and its properties that emerge from QCD to obtain a description based on first principles. In the QCD phase diagram, shown in Figure 1, the QGP lies in the high temperature T and high baryochemical potential μ_B regime, at least one of them is needed to enter the QGP phase. The baryochemical potential μ_B is a measure of the imbalance of matter and anti-matter, it is zero if the same amount of both are present. Large baryochemical potentials are believed to be found in neutron stars, but they are not accessible to physical study yet.

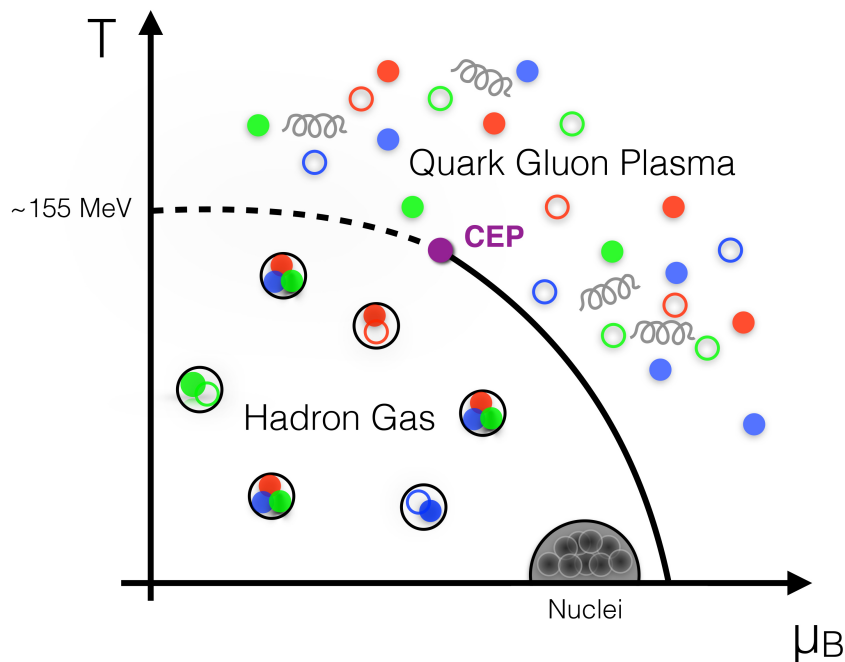


Figure 1: QCD phase diagram in temperature and baryochemical potential [29]

The region in the QCD phase diagram that is accessible today is the high temperature regime. Current Lattice QCD calculations [29] estimate a critical temperature of approximate $T_c = 155$ MeV, which corresponds to a value of about 1.8×10^{12} K. In this region, the transition from the HG phase to the QGP phase is a continuous crossover, which is shown as a dashed line in Figure 1. The high temperature regime is reached in ultra-relativistic heavy-ion collisions using particle accelerators, where ion beams are accelerated to velocities near the speed of light and initial collision temperatures of about 300 – 600 MeV can be obtained. The dedicated heavy-ion detector at the LHC at CERN [32], the European Organization for Nuclear Research, is ALICE (A Large Ion Collider Experiment) [33]. At ALICE, millions of events from lead-lead collisions with a centre-of-mass energy of 2.76 TeV per nucleon pair were recorded in 2010/2011. An example of such an event is shown in Figure 2, the red lines are the reconstructed charged particle tracks. One can easily see that the particle tracks are not all in the same direction but instead show an angular distribution.

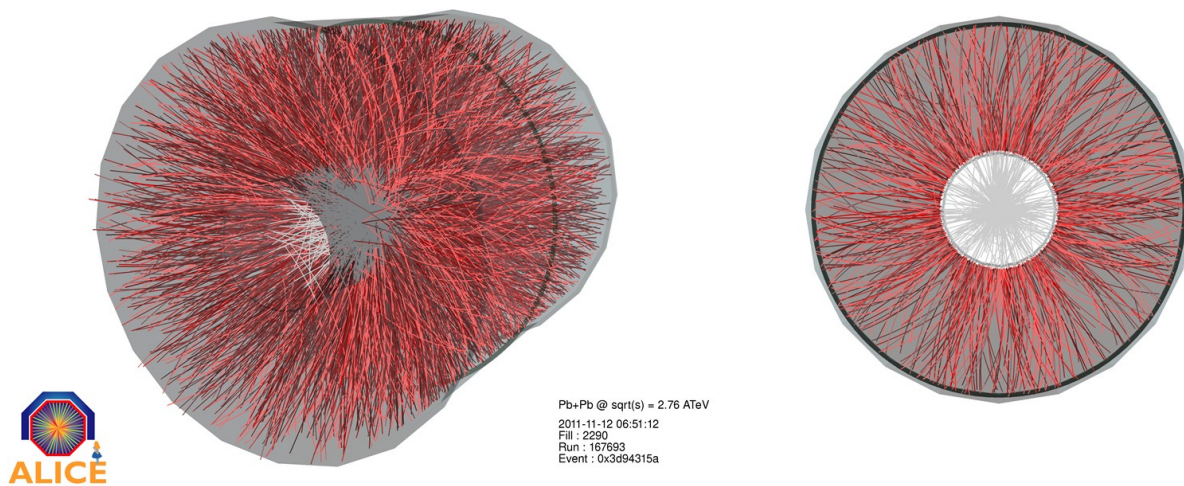


Figure 2: Events recorded by ALICE from the first lead ion collisions in 2011 [34]

The momentum p of a particle can be divided into components parallel p_L and transverse p_T to the beam axis. The angle between the momentum p and the beam axis is called θ . The transverse momentum p_T and longitudinal momentum p_L can then be expressed by:

$$p_T = p \sin \theta \quad (1)$$

$$p_L = p \cos \theta \quad (2)$$

The velocity v of the particles in units of the speed of light c is:

$$\beta = \frac{v}{c} \quad (3)$$

One can now introduce a quantity called rapidity y , which has the transformation property that it changes only by an additive constant in a frame of reference moving in relation to the original one. The rapidity y is given by:

$$y = \frac{1}{2} \ln \left(\frac{E + p_L}{E - p_L} \right) = \frac{1}{2} \ln \left(\frac{1 + \beta_L}{1 - \beta_L} \right) = \operatorname{arctanh} \beta_L \quad (4)$$

with L indicating the longitudinal component and the relativistic energy-momentum relation (in heavy-ion physics, one commonly uses natural units, i.e. $\hbar = c = k_B = 1$):

$$E^2 = p^2 + m^2 \quad (5)$$

For the ultra-relativistic case where the momentum p is much higher than the particle's rest mass m , $p \gg m$, the rapidity is equal to a quantity that solely depends on the measured angle θ , the pseudorapidity η :

$$\eta = -\ln \tan \frac{\theta}{2} \quad (6)$$

By counting the number of particles within a given pseudorapidity range in each event, we can compute the charged particle multiplicity $dN_{ch}/d\eta$. This is done at large scale at ALICE, where the detectors are able to process millions of events with thousands of produced charged particles each. Of course, there is additional information to be obtained through specific detection methods, which make it possible to, for example, determine the time of flight, reconstruct the particle trajectory and identify the particles by their specific energy loss, i.e. answer the question if the measured charged particle was e.g. a pion, kaon, proton or electron. These tasks are performed by the TOF (Time Of Flight), ITS (Inner Tracking System) and TPC (Time Projection Chamber). The ALICE detector setup is shown in Figure 3. For a detailed description of the ALICE experiment, I refer the reader to the ALICE Collaboration [36].

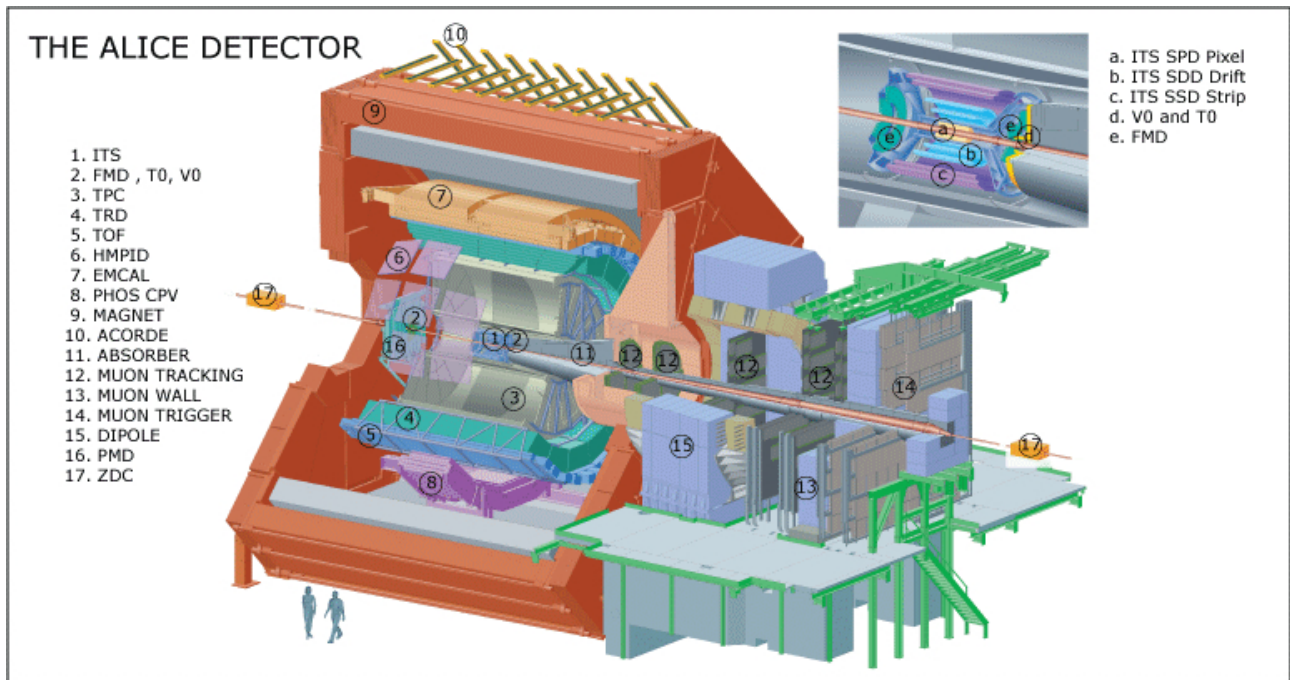


Figure 3: ALICE detector setup [33]

Using this detector data, one can determine the rapidity y and transverse momentum p_T of the identified particles and compute their invariant yield $E \frac{d^3N}{dp^3}$. The invariant yield has the property of Lorentz invariance, so its value does not change in a boosted frame of reference. It can be experimentally computed by:

$$E \frac{d^3N}{dp^3} = \frac{1}{2\pi p_T} \frac{d^2N}{dy dp_T} \quad (7)$$

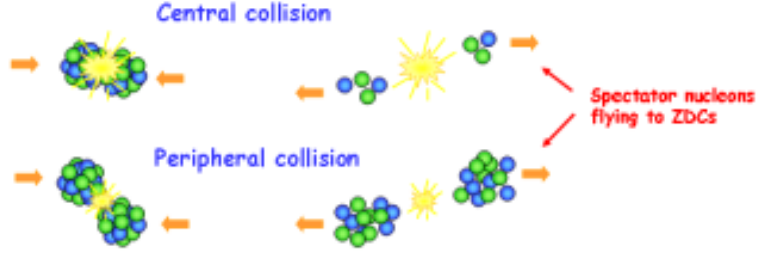


Figure 4: central collision compared to peripheral collision [33]

The data used as input to the first method in Sec. 2 consists of the invariant yields of different particle species (π , K, p, Λ , Ξ , Ω) in the low p_T range. The data is divided into different classes according to the centrality of the collisions. A central collision has a high number of nucleons that participate in the collision while a peripheral collision has a low number of nucleons that participate in the collision, this is illustrated in Figure 4. In the ALICE experiment, the centrality is measured by the ZDC (Zero Degree Calorimeters) detector shown in Figure 3, which is able to detect the energy of the non-participating nucleons. The centrality class of the data used for the computations in Sec. 2 is 0 – 10%, meaning that the 10% most central collisions are included.

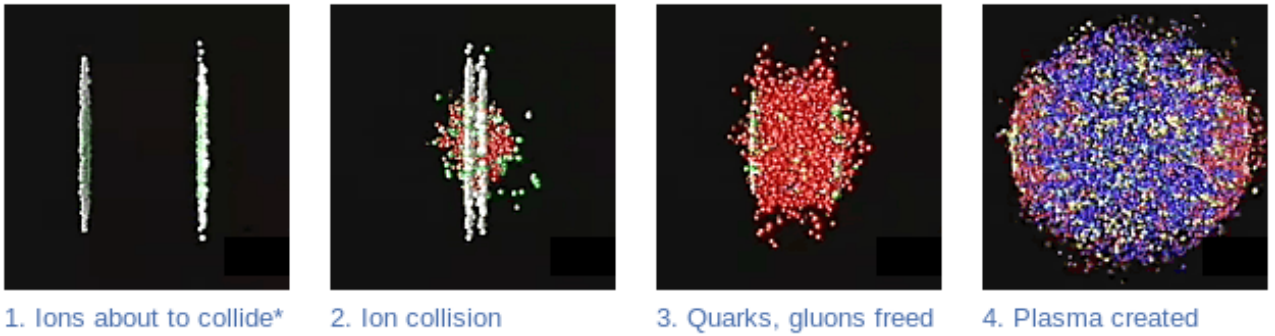


Figure 5: relativistic heavy-ion collision [35]

A heavy-ion collision is expected to look as in the simulation shown in Figure 5. The ions that are about to collide are Lorentz-contracted, i.e. their width is compressed due to their velocity being near the speed of light. The ions then collide, high initial temperatures are produced due to the high collision energy and a fast thermalization happens. If the produced temperature exceeds the critical temperature needed to transition into the QGP phase, see Figure 1, which is expected for ultra-relativistic heavy-ion collisions, the quarks and gluons are freed and so the QGP is created. The dynamics of the QGP phase can with great success be described by (nearly) ideal relativistic hydrodynamics, meaning one can imagine the QGP as an expanding fluid. The expanding QGP cools off and thousands of hadrons are produced from the formerly deconfined quarks. The space-time evolution of this process is shown in Figure 6. At $t < 0$, the heavy-ion beams are about to collide. After the collision at $t = 0$, a formation phase takes place and at $t \approx 1 - 2$ fm/c, the QGP phase is entered. The plasma expands in space and over time cools off. When the temperature has lowered to the critical temperature T_c after $t \approx 10$ fm/c, the chemical freezeout occurs at $T_{ch} \approx T_c$, i.e. inelastic processes cease and the QGP makes its crossover to the HG phase. The HG phase freezes out kinetically at $T_{fo} \approx 100$ MeV, which means that the hadron momenta stop changing, and further cools off.

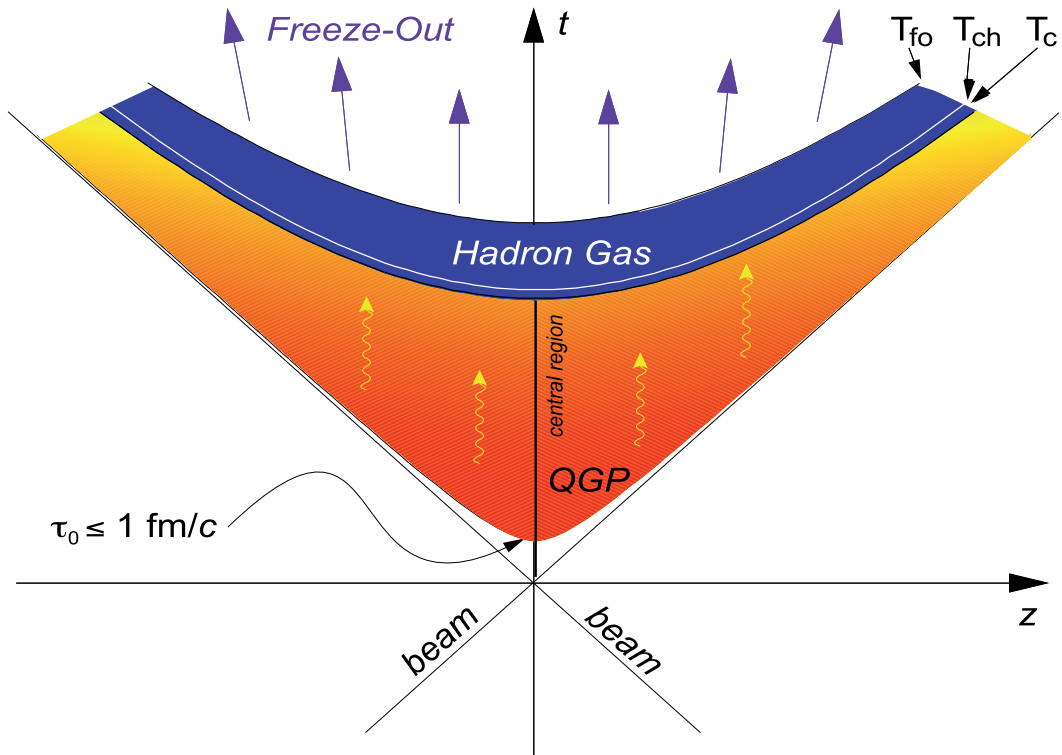


Figure 6: space time evolution of a relativistic heavy-ion collision [31]

According to the big bang theory, the early universe is expected to have also transitioned from the QGP phase into the hadron gas phase at a time of $\approx 10^{-5}$ seconds after the big bang. Shortly after the big bang, the universe was in a state of extremely high temperature and density and ≈ 0 baryochemical potential, which puts it into the same region in the QCD phase diagram as achieved in heavy-ion collisions by particle accelerators like the LHC today, see Figure 1. This makes the investigation of the QGP particularly interesting because at the same time one investigates the properties of the early universe, as both are examples of QCD in the non-perturbative regime of ultra-high temperature and density. Success in obtaining the characteristics of the QGP from first-principle QCD calculations would dramatically enrich our knowledge about the evolution of the early universe. A simple comparison between the evolution of the fireball formed in heavy-ion collisions and that of the big bang is shown in Figure 7. There are two important differences:

- The formation time τ of the QGP is different because during the big bang, gravity had an extremely strong influence on the speed of expansion of the fireball and slowed it down by many orders of magnitude. This allowed for interactions and formation of structures in the mixed phase of the QGP and the HG phase which are not possible during heavy-ion collisions.
- There is a larger matter-antimatter asymmetry in heavy-ion collisions than there was at the big bang because the heavy-ion collisions are created with an initial baryon number N_b , which is more significant compared to the final particle number N .

While one is not able to reproduce the slow evolution of the big bang experimentally, the matter-antimatter asymmetry is reduced by moving to higher center-of-mass energies, such that in my analysis with data from central lead-lead collisions at $\sqrt{s_{NN}} = 2.76$ TeV, I am able to neglect the matter-antimatter asymmetry. By analyzing ultra-relativistic heavy-ion collisions, one aims to understand how the process of hadronization took place in the early universe.

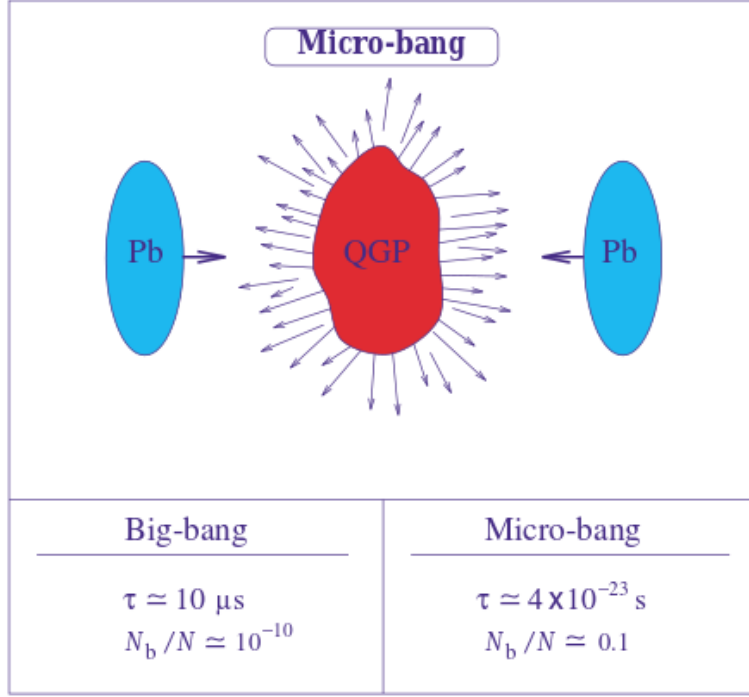


Figure 7: ultra-relativistic lead-lead collision (micro-bang) and big bang [7]

1.2 Motivation

The motivation of my thesis is the paper *Parametric estimate of the relative photon yields from the Glasma and the Quark-Gluon Plasma in heavy-ion collisions* [12] by J. Berges, K. Reygers, N. Tanji and R. Venugopalan, where the coefficients c_{eq} and c_T that are related to the thermalization time and its initial temperature are estimated. During the computation for this estimation, the charged particle multiplicity has to be converted to the entropy of the hadrons per pseudorapidity, which is done by the factor $k_{S/N}$ from Eq. (49) in Ref. [12]:

$$\frac{dS_{\text{hadron}}}{d\eta} = k_{S/N} \frac{dN_{ch}}{d\eta} \quad (8)$$

$$\frac{S}{N_{ch}} = k_{S/N} = \frac{dS_{\text{hadron}}}{d\eta} / \frac{dN_{ch}}{d\eta} \quad (9)$$

Because S/N_{ch} is not available for Pb-Pb collisions at $\sqrt{s_{NN}} = 2.76 \text{ TeV}$ at the LHC, the authors used the value $S/N_{ch} = 7.2$ for Au-Au collisions at $\sqrt{s} = 130 \text{ A GeV}$ at RHIC provided by Subrata Pal and Scott Pratt in *Entropy Production at RHIC* [1]. In my thesis, I will provide the LHC value and compare it to the result of Pal and Pratt.

1.3 Methods for entropy estimation

1.3.1 Entropy from Bjorken flow

In the paper *Entropy production in collisions of gravitational shock waves and of heavy ions* [13] by Steven S. Gubser, Silviu S. Pufu, Amos Yarom, the authors use three approaches to estimate the entropy.

The first approach is to estimate the entropy from Bjorken flow. A basic assumption is that the entropy per charged particle does not change significantly with rapidity, i.e.:

$$\frac{S}{N_{\text{charged}}} \approx \left. \frac{dS/dy}{dN_{\text{charged}}/dy} \right|_{\text{midrapidity}} \quad (10)$$

From the Bjorken treatment [15], they get the relations:

$$\tau_{\text{form}} A \epsilon(\tau_{\text{form}}) = \frac{dE_T}{dy} \quad (11)$$

$$\tau_{\text{form}} A s(\tau_{\text{form}}) = \frac{dS}{dy} \quad (12)$$

with formation time τ_{form} , temperature T , cross-sectional area A , energy density ϵ , entropy density s and transverse energy E_T . Assuming the QGP is a thermalized plasma at formation time

$$s = \frac{4}{3} \frac{\epsilon}{T} \quad (13)$$

and combining the relations above, the authors get their resulting formula:

$$\frac{dS}{dy} = \frac{4}{3T} \frac{dE_T}{dy} \quad (14)$$

For central Au-Au collisions at $\sqrt{s_{NN}} = 200$ GeV, Gubser, Pufu et al. estimate a transverse energy density of $dE_T(\tau_{\text{form}})/dy \approx dE_T(\text{final})/d\eta \approx 600$ GeV. Also, they choose the values for the formation time $\tau_{\text{form}} = 1$ fm and cross-sectional area $A = 120$ fm², which gives them a temperature of $T = 240$ MeV and their result for dS/dy :

$$\frac{dS(\tau_{\text{form}})}{dy} \approx 3300 \quad (15)$$

Using the RHIC value $dN_{\text{charged}}/dy \approx 660$ for central collision near mid-rapidity [16], the authors arrive at:

$$\frac{dS(\tau_{\text{form}})}{dy} \approx 5 \frac{dN_{\text{charged}}}{dy} \quad (16)$$

which, using Eq. 10 and $N_{\text{charged}} \approx 5000$ [16] for central collisions, leads to:

$$S \approx 5 N_{\text{charged}} \approx 25000 \quad (17)$$

$$\frac{S}{N_{ch}} \approx 5 \quad (18)$$

For this approach, Gubser, Pufu et al. note that it provides only a rough estimate of entropy because many approximations were used. For more accurate results, different approaches are recommended.

1.3.2 Entropy from phase space density

The second approach is to estimate the entropy from phase space density. The entropy S and number of hadrons N are given by summing over all known hadron resonances, neglecting interactions among hadrons:

$$S = \sum_i \int \frac{d^3x d^3p}{(2\pi^3)} [-f_i \log f_i \pm (1 \pm f_i) \log (1 \pm f_i)] \quad (19)$$

$$N = \sum_i \int \frac{d^3x d^3p}{(2\pi^3)} f_i \quad (20)$$

with upper (lower) sign for bosons (fermions), and phase space density f_i :

$$f_i = \frac{1}{\exp \sqrt{p^2 + m_i^2}/T \mp 1} \quad (21)$$

with $T = 170$ MeV. This leads to the result:

$$\frac{S}{N} = 5.15 \quad (22)$$

Gubser, Pufu et al. use $N/N_{ch} = 1.5$ to get the entropy per number of charged particles. These values for S/N and N/N_{ch} are also noted in the paper *Possible Resolutions of the D-Paradox* [20] by C. Nonaka, B. Müller et al. One gets for the entropy per charged hadron:

$$\frac{S}{N_{ch}} = 7.7 \quad (23)$$

The authors note that this estimation is only approximate because of the neglect of chemical potentials and could be improved by using available data for dS/dy and $dN_{charged}/dy$. That method was introduced by Subrata Pal and Scott Pratt in their paper *Entropy Production at RHIC* [1] and I explain it in detail in Sec. 2, where I also apply it to Pb-Pb collisions at $\sqrt{s_{NN}} = 2.76$ TeV at the LHC.

The difference in the method of Pal and Pratt lies in using experimental data to estimate the phase space density instead of using Eq. 21. For Au-Au collisions at $\sqrt{s_{NN}} = 130$ GeV at RHIC, one gets from Ref. [17]:

$$\frac{dN_{ch}}{dy} \approx 620 \quad (24)$$

Pal and Pratt's result [1] for the entropy rapidity density is:

$$\frac{dS}{dy} = 4451 \pm 10\% \quad (25)$$

which leads to an entropy per number of charged particles of:

$$\frac{S}{N_{ch}} \approx \frac{dS/dy}{dN_{ch}/dy} = 7.2 \quad (26)$$

Finally, Gubser, Pufu et al. take the average of Eq. 23 and Eq. 26 to arrive at their result:

$$\frac{S}{N_{ch}} = 7.5 \quad (27)$$

1.3.3 Entropy from immediate equilibration

The third approach is to estimate the entropy from immediate equilibration using the Landau model [18], assuming the validity of hydrodynamics and the equation of state $\epsilon = 3p$. First, the total energy E_{tot} is calculated by:

$$E_{tot} = \frac{N_{\text{part}} \sqrt{s_{NN}}}{2} \quad (28)$$

With $\sqrt{s_{NN}} = 200$ GeV and estimating $N_{\text{part}} = 350$ for the number of participants in the 5% most central collisions, one gets a total energy of 35 TeV. The authors state that the nuclei have a volume of about $V = 4/3 \pi (6.5 \text{ fm})^3$ in their rest frame that is flattened by the factor $\gamma = \sqrt{s_{NN}}/2m_{\text{proton}}$ in the lab frame, which leads to the following energy density ϵ of overlapping colliding nuclei:

$$\epsilon = \frac{\gamma E_{tot}}{V} = 3300 \text{ GeV/fm}^3 \quad (29)$$

Using the results of the lattice QCD calculations done in Ref. [19], Fig. 1,

$$\frac{\epsilon}{T^4} \approx 11 \quad (30)$$

for $1.2 T_c \leq T \leq 2 T_c$, one gets a temperature of $T = 1200$ MeV. The entropy can now be calculated by:

$$S = \frac{4 E_{tot}}{3 T} \approx 38000 \quad (31)$$

Note: This formula implies a scaling of the entropy with the center-of-mass energy of $S \propto s^{1/4}$ but the recent value for heavy-ion collisions extracted from measurements is $S \propto s^{0.155}$ [24]. With $N_{\text{charged}} \approx 5000$ for central collisions from Ref. [16], Gubser, Pufu et al. then arrive at the same result as in their previous approach, see Eq. 27:

$$\frac{S}{N_{ch}} = 7.5 \quad (32)$$

1.3.4 Entropy from hadron resonance gas model

In the paper *From Entropy and Jet Quenching to Deconfinement?* [14] by Berndt Müller and Krishna Rajagopal, the authors estimate the entropy by analyzing the composition of the fireball at chemical freezeout using a hadron resonance gas model, which is my second method for entropy estimation, and is described in detail in Sec. 3. Müller and Rajagopal use a chemical freezeout temperature of $T_{ch} = 170 \pm 10$ MeV to model an ideal gas of all meson and baryon resonances found in the Particle Data Group [11] (2005) and get an entropy per hadron of:

$$\frac{S}{N} = 7.25 \quad (33)$$

The authors state that after all resonance decays, the number of hadrons per number of charged hadrons in the final state is:

$$\frac{N}{N_{ch}} = \frac{1}{1.04} \quad (34)$$

This corresponds to a value of $S/N_{ch} = 6.97$. The entropy per hadron of an ideal hadron gas is dependent on temperature, so the choice of the chemical freezeout temperature introduces an

uncertainty into S/N . Müller and Rajagopal calculated that an uncertainty in temperature of 10 MeV leads to an uncertainty in the entropy per hadron of 3%. An additional uncertainty comes from neglecting the width of states, this also leads to an uncertainty of 3%. Also, there may be resonances that were not included in the particle list, but as the authors observe, the value for S/N converges rather fast to its final value, so neglecting a portion of high mass resonances does not result in a significant deviation of the result.

1.3.5 Entropy from thermal model

In the paper *Investigation of Hadron Multiplicities and Hadron Yield Ratios in Heavy Ion Collisions* [21] by D.R. Oliinychenko, K.A. Bugaev and A.S. Sorin, a thermal model similar to that described in Ref. [22] is used to estimate the entropy per hadron. In the thermal model, the central equation is the partition function of the grand canonical ensemble, which is given by:

$$\ln Z_i = \frac{V g_i}{2\pi^2} \int_0^\infty \pm p^2 dp \ln[1 \pm \exp(-(E_i - \mu_i)/T)] \quad (35)$$

with index i for a given particle species, $g_i = 2J_i + 1$, energy $E_i = \sqrt{p^2 + m_i^2}$ with mass m_i , temperature T and chemical potential μ_i , compounded by the potentials related to baryon number, isospin, strangeness and charm, ensuring conservation of the quantum numbers, the upper sign is for fermions and the lower sign for bosons. One then gets for the number of particles per volume:

$$n_i = \frac{g_i}{2\pi^2} \int_0^\infty \frac{p^2 dp}{\exp(-(E_i - \mu_i)/T) \pm 1} \quad (36)$$

The authors use the data from their own parametrization of the thermal model together with the data extracted from Ref. [22] to compute the entropy per hadron over a large $\sqrt{s_{NN}}$ range and observe a nearly constant behavior for S/N over the whole range. From this, they conclude that the entropy per hadron is a robust chemical freezeout criterion. As resulting value, Oliinychenko, Bugaev and Sorin obtain by fitting:

$$\frac{S}{N} = 7.16 \pm 8\% \quad (37)$$

1.3.6 Entropy from interacting hadron gas model

In the paper *Interacting hadron resonance gas meets lattice QCD* [23] by A. Andronic, P. Braun-Munzinger et al. the authors use an interacting hadron gas model to compute different thermodynamical quantities, including the entropy density s and the number density n of mesons and baryons. The central model equations are identical to that described in Sec. 1.3.5. The authors use a critical temperature of $T = 164$ MeV and a baryochemical potential of $\mu_b = 0.8$ MeV, which are their expected values at LHC energy. Their particle list includes all known mesons and baryons up to 3 GeV from the PDG [11] (2008), the width of states is included in their model. The interaction part of the model is done by an excluded volume correction, meaning that the hadrons occupy a finite volume. From Figure 6 in Ref. [23], I extract the following values for the entropy per hadron (indices: m for meson, b for baryon):

$$\frac{S}{N} = \frac{s}{n_m + n_b} = 7.28 \text{ (without volume correction: } R_m = R_b = 0) \quad (38)$$

$$\frac{S}{N} = \frac{s}{n_m + n_b} = 7.61 \text{ (with volume correction: } R_m = R_b = 0.3 \text{ fm)} \quad (39)$$

2 Entropy estimation according to Pal and Pratt

The first method to estimate the final-state entropy for Pb-Pb collisions at $\sqrt{s_{NN}} = 2.76$ TeV at the LHC (centrality 0 – 10%) follows the method used by Subrata Pal, Scott Pratt to estimate the final-state entropy for Au-Au collisions at $\sqrt{s} = 130$ A GeV at RHIC in their paper *Entropy Production at RHIC* [1]. This method uses solely the measured particle spectra and HBT radii of different particle species to estimate their entropy per unit rapidity at freeze-out. The important quantity is the phase space density $f(\mathbf{p}, \mathbf{r}, t_f)$ with freezeout time t_f . Because the particle spectra only provide information about the momenta \mathbf{p} , one has to relate them to the phase space density and the radii \mathbf{r} . For the radii, for $t \geq t_f$, Pal and Pratt assume a three-dimensional Gaussian. The phase space density then becomes:

$$f(\mathbf{p}, \mathbf{r}, t) = f_{\max}(\mathbf{p}) \exp\left(-\sum_{i=1}^3 \frac{x_i^2}{2R_{x_i}^2}\right) \quad (40)$$

The measured particle spectra result from integrating the phase space density, so one can obtain $f_{\max}(\mathbf{p})$ from the spectra by computing:

$$\frac{d^3N}{dp^3} = (2J + 1) \int \frac{d^3r}{(2\pi)^3} f(\mathbf{r}, \mathbf{p}) \quad (41)$$

$$f_{\max}(\mathbf{p}) = \frac{(2\pi)^{3/2} d^3N}{2J + 1} \frac{1}{dp^3 \prod_{i=1}^3 R_i} \quad (42)$$

To get the radii, one has to take the interaction between two particles that were emitted independently from the same source region into account, these are the so called *Hanbury-Brown-Twiss Correlations* [25]. The two-particle correlations are described by the correlation function $C_2(\mathbf{q}, \mathbf{K})$ [26],[27],[1]:

$$C_2(\mathbf{q}, \mathbf{K}) = \frac{d^6N/(d^3k_1 d^3k_2)}{(d^3N/d^3k_1)(d^3N/d^3k_2)} = \frac{P(k_1, k_2)}{P(k_1)P(k_2)} = 1 + |\tilde{\rho}(\mathbf{q})|^2 \quad (43)$$

with $\mathbf{q} = k_1 - k_2$, $\mathbf{K} = (k_1 + k_2)/2$ and $\tilde{\rho}$ the Fourier transform of the spatial distribution of the particle source. C_2 is then parametrized using the Bertsch-Pratt variables q_{out} , q_{side} , q_{long} [28], where q_{long} points along the beam axis, q_{out} parallel to the transverse component of \mathbf{K} and q_{side} is orthogonal to both. For a Gaussian source and using this parametrization, the correlation function can be expressed by:

$$C_2(q_{\text{out}}, q_{\text{side}}, q_{\text{long}}) = 1 + \exp(-R_{\text{out}}^2 q_{\text{out}}^2 - R_{\text{side}}^2 q_{\text{side}}^2 - R_{\text{long}}^2 q_{\text{long}}^2) \quad (44)$$

A schematic representation of the radii is shown in Figure 8. With Eq. 44, the product of the radii in Eq. 42 then becomes:

$$\prod_{i=1}^3 R_i = R_{\text{inv}}^3 = \gamma R_{\text{out}} R_{\text{side}} R_{\text{long}} \quad (45)$$

with the gamma factor $\gamma = E_T/m$ because of the Lorentz-contraction in the data analysis frame compared to the two-particle rest frame.

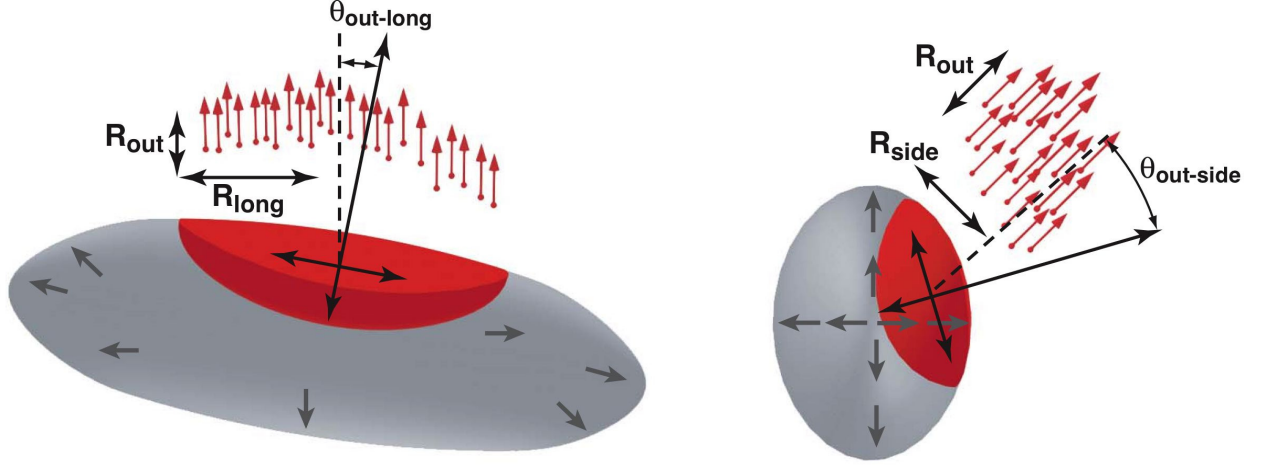


Figure 8: orientation of the out-side-long axes for a viewer perpendicular (left) and parallel (right) to the beam axis [26]

Pal and Pratt now replace the discrete-level sum and use the classical limit of the entropy from phase space density introduced in Sec. 1.3.2 to get the entropy of a given particle species with spin quantum number J :

$$S = \sum_i \int \frac{d^3r d^3p}{(2\pi^3)} [-f_i \ln f_i \pm (1 \pm f_i) \ln (1 \pm f_i)] \quad (46)$$

$$S \approx (2J + 1) \int \frac{d^3r d^3p}{(2\pi)^3} [-f \ln f + f \pm f^2/2] \quad (47)$$

with positive sign for bosons and negative sign for fermions.

Finally, the entropy per unit rapidity is obtained by combining Eqs. 40, 42, 45, 47:

$$\frac{dS}{dy} = \int dp_T 2\pi p_T E \frac{d^3N}{dp^3} \left(\frac{5}{2} - \ln \mathcal{F} \pm \frac{\mathcal{F}}{2^{5/2}} \right) \quad (48)$$

with:

$$\mathcal{F} = \frac{1}{m} \frac{(2\pi)^{3/2}}{2J + 1} \frac{1}{R_{inv}^3} E \frac{d^3N}{dp^3} \quad (49)$$

with degeneracy $g = 2J + 1$, particle mass m , the sign is $+$ for bosons and $-$ for fermions. The R_{inv} data is fit by:

$$R_{inv}(p_T) = \frac{R_0}{\sqrt{m_T}} \quad (50)$$

with $m_T = \sqrt{p_T^2 + m^2}$ and particle mass m . Pal and Pratt use the HBT radius of \bar{p} for all baryons and anti-baryons. The entropy rapidity density has to be separately calculated for each particle species one wants to consider for the final-state entropy. The important question here lies in what particles are important to include for a meaningful estimation the final-state entropy. So first, I reconstruct the way Pal and Pratt computed their result in Table 1.

Table 1: Reconstructing Pal and Pratt's result

particle	dS/dy one charge	factor	dS/dy total
π	680	3	2040
η			256
η'			69
K^-			256
K^+			286
$K^0 + \bar{K}^0$			542
\bar{p}			118
p			159
$\bar{\Lambda} + \bar{\Sigma}^0$			81
$\Lambda + \Sigma^0$			111
$\bar{\Sigma}^\pm$	31	2	62
Σ^\pm	42	2	84
$\bar{\Xi}^\pm + \bar{\Xi}^0$	23	2	46
$\Xi^- + \Xi^0$	27	2	54
$\Omega^- + \bar{\Omega}^+$			10
$n + \bar{n}$			277
total sum			4451

They use the particle spectra for the $\approx 11\%$ most central Au-Au collisions at midrapidity at the RHIC energy of $\sqrt{s} = 130$ A GeV. For the $n + \bar{n}$, Pal and Pratt use the entropy rapidity density of the $p + \bar{p}$, for the η , they use the K^- because of the similar mass. For the η' , they argue that it contributes an entropy of half of the average of p and \bar{p} , because of the lower spin degeneracy. The entropy $K^0 + \bar{K}^0$ is assumed to be equal to that of $K^- + K^+$. For the anti-baryons, the yield ratio is used as a correction (note: for LHC energy, one can neglect this correction because the baryochemical potential $\mu_B \approx 0$). The Σ are extracted via the thermodynamical model (explained in Sec. 3) using:

$$N = \sum_{k=1}^{\infty} \frac{Tg}{2\pi^2} \frac{(\text{sign})^{k+1}}{k} m^2 \mathcal{K}_2 \left(\frac{km}{T} \right) \exp \frac{\mu_B}{T} \quad (51)$$

with degeneracy $g = 2J + 1$, temperature $T = 173$ MeV, particle mass m , baryochemical potential μ_B and Bessel function \mathcal{K}_n of kind n , the sign is + for bosons and - for fermions. (Note: I will use a baryochemical potential of $\mu_B \approx 0$ and a temperature of $T = 156$ MeV during my calculations for LHC energies.)

The result of Pal and Pratt is shown in Figure 9. They estimate $\epsilon_0 = 7 \pm 2$ GeV/fm³ for the energy density at $\tau = 1$ fm/c and a systematic uncertainty of their result of 10% from the uncertainty of the measured yields. The Bjorken energy density ϵ_{Bj} is used as a lower bound. One can see that their result is in agreement with their Lattice QCD calculations.

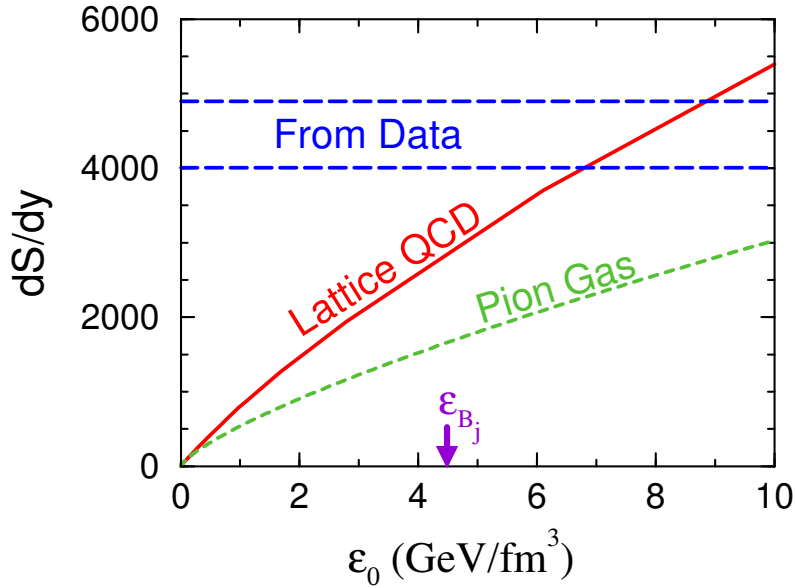


Figure 9: result of Pal and Pratt [1]

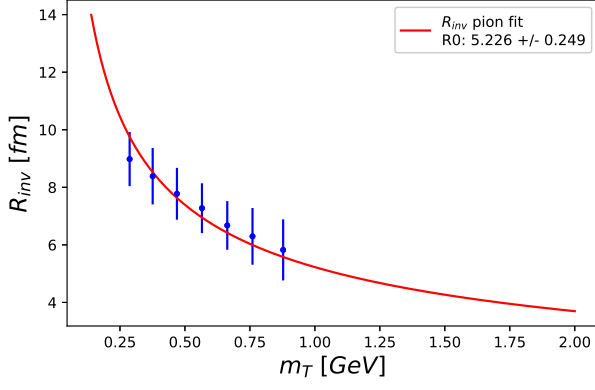
Pal and Pratt's result for the final-state entropy for Au-Au collisions at $\sqrt{s} = 130$ A GeV at RHIC is:

$$\boxed{\frac{dS}{dy} = 4451 \pm 10\%} \quad (52)$$

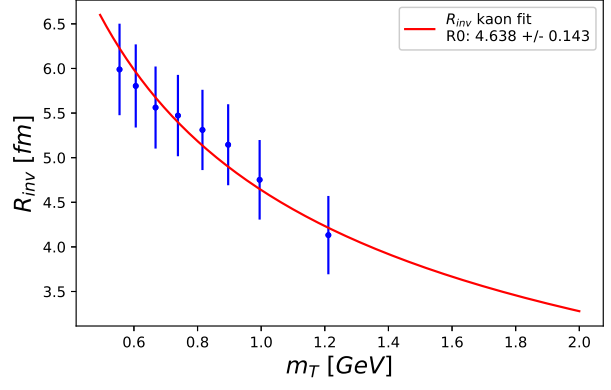
Now, that I have reconstructed Pal and Pratt's result for Au-Au collisions at $\sqrt{s} = 130$ A GeV at RHIC, I can begin following their recipe to estimate the final-state entropy for Pb-Pb collisions at $\sqrt{s_{NN}} = 2.76$ TeV at the LHC.

For my computations, I use particle spectra measured by ALICE in Pb-Pb collisions at $\sqrt{s_{NN}} = 2.76$ TeV with a centrality of 0 – 10%. The π , K and p data are from the ALICE Collaboration 1303.0737 [2], the Ξ and Ω data from the ALICE Collaboration 1307.5543 [3] and the Λ data from the ALICE Collaboration 1307.5530 [4]. The R_{inv} data is from the ALICE Collaboration 1506.07884 [5].

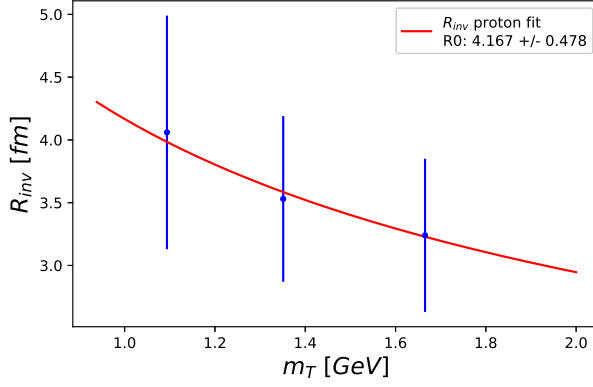
For the HBT radii, I fit Eq. 50 to the data. The R_{inv} data available to me only covers π , K and p , so, following Pal and Pratt's approach, as they use the HBT radius of \bar{p} for all baryons and anti-baryons, I use the HBT radius of p for the remaining baryons, i.e. for Λ , Ξ and Ω . The fits to the R_{inv} data are shown in Figure 10.



(a) R_{inv} π fit



(b) R_{inv} K fit



(c) R_{inv} p fit

Figure 10: R_{inv} fits

To calculate dS/dy with Eq. 48, one theoretically has to integrate over the complete p_T range, but the available data of course cannot provide this. Because the invariant yields go to 0 for $p_T \rightarrow \infty$, the data covers enough of the high p_T range, as one can always spot the convergence to zero. For the low p_T range, one cannot neglect the particle yield below the range of the measurement, so I extrapolate the data to $p_T = 0$ using different fit functions. The fits to the invariant yields are then only used in the low p_T region, where no data is available, otherwise the integration is performed over the available data. The invariant yields of each particle species are fit by four different functions to also account for the systematic uncertainty resulting from the fit model selection. A similar approach is described in Ref. [2], page 15, where $dN_{ch}/d\eta$ is calculated, which I will also use as a crosscheck for my results. The fit functions I use are the Bose-Einstein (53), Tsallis-Levy (54), m_T exponential (55) and Boltzmann (56) distributions.

Bose-Einstein:

$$f(p_T) = \frac{A}{\exp\left(\sqrt{p_T^2 + m^2}/T\right) - 1} \quad (53)$$

Tsallis-Levy:

$$f(p_T) = \frac{A}{2\pi nC[nC + m(n-2)]} \left(1 + \frac{\sqrt{p_T^2 + m^2} - m}{nC}\right)^{-n} \quad (54)$$

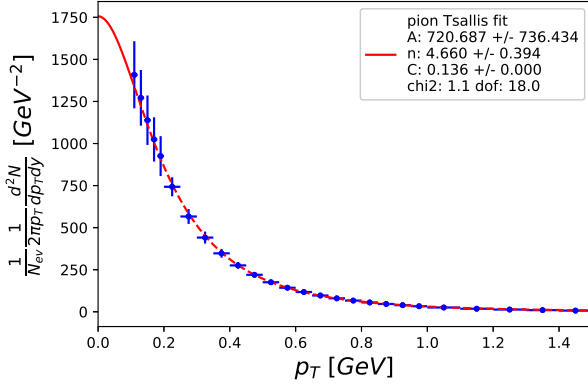
m_T exponential:

$$f(p_T) = A \exp\left(\frac{-\sqrt{p_T^2 + m^2}}{T}\right) \quad (55)$$

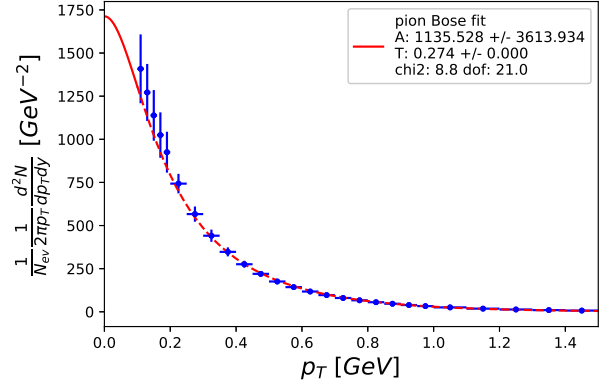
Boltzmann:

$$f(p_T) = A \sqrt{p_T^2 + m^2} \exp\left(\frac{-\sqrt{p_T^2 + m^2}}{T}\right) \quad (56)$$

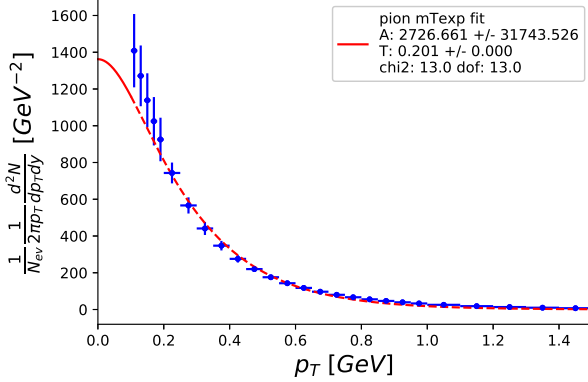
with transverse momentum p_T and particle mass m . The fit parameters for Bose-Einstein, m_T exponential and Boltzmann distributions are A and T , and for Tsallis-Levy distribution A , n and C . The fits to the invariant yields of my considered particles, i.e. π , K , p , Λ , Ξ and Ω , are shown in full for π in Figure 11 and for each of the other particle species, a selected fit is shown in Figure 12. A complete overview of all fits is provided in the appendix, Figure 18-23.



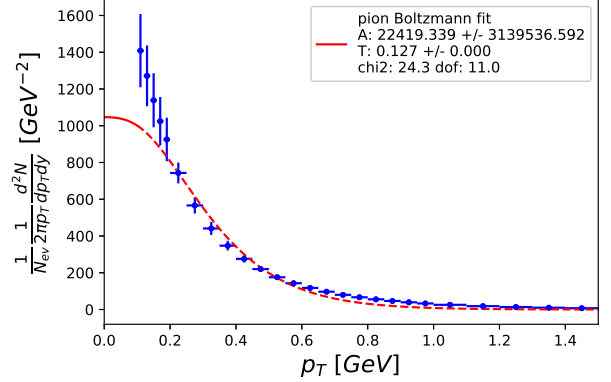
(a) π Tsallis fit



(b) π Bose fit



(c) π m_T exp fit

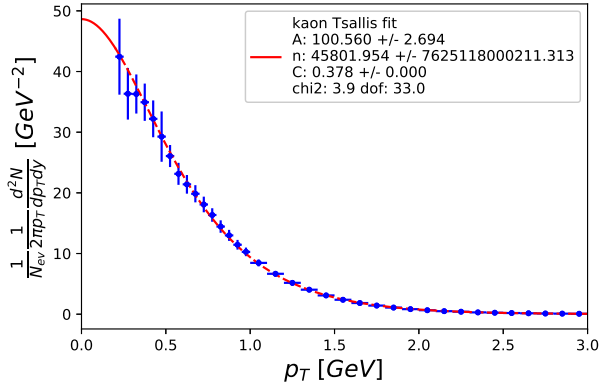


(d) π Boltzmann fit

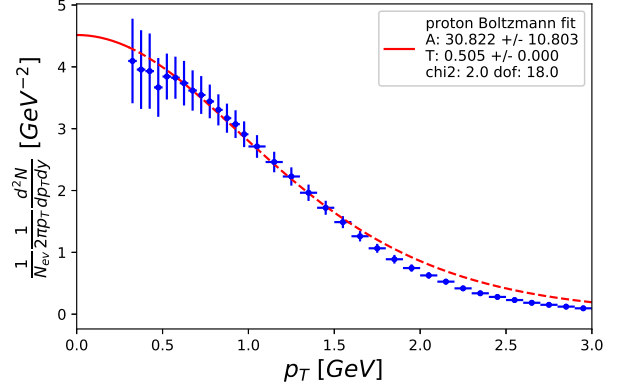
Figure 11: π fits

The estimation of the uncertainties is done with Monte Carlo error propagation, using the statistical and systematic uncertainty of the data over the available range, and the uncertainty of the fit parameters for the extrapolation to $p_T \rightarrow 0$. With this, dS/dy is calculated in many trials and I obtain its error by the square root of the variance of all trial values. Also, the variance of the value for dS/dy caused by using four different fit functions for the data extrapolation provides an additional systematic uncertainty.

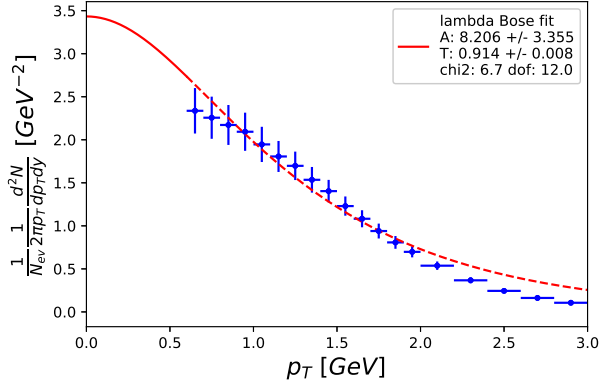
Now, I crosscheck my approach with that used in Ref. [2] for dN_{ch}/dy and calculate dN_{ch}/dy for each particle species. This is a meaningful crosscheck because we both use the same data for



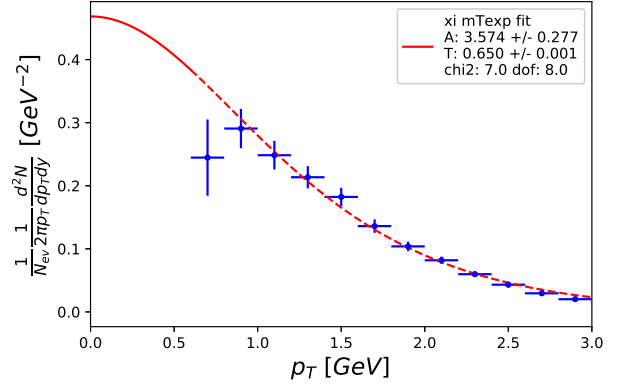
(a) K Tsallis fit



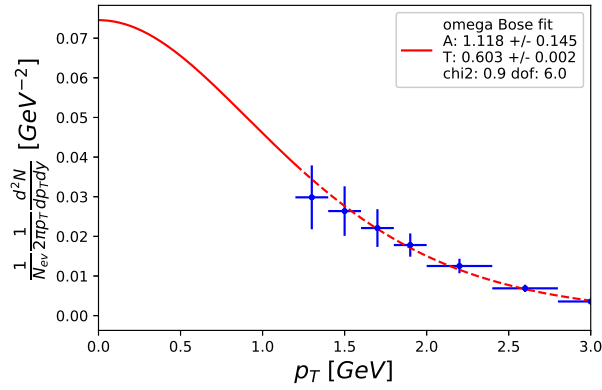
(b) p Boltzmann fit



(c) Λ Bose fit



(d) Ξ m_T exp fit



(e) Ω Bose fit

Figure 12: selected K , p , Λ , Ξ , Ω fits

π , K and p in our model and for both dN_{ch}/dy and dS/dy , one has to do an integration where a correct handling of the invariant yield, its uncertainty estimation and data extrapolation are the significant challenges in getting a convincing result. If this works correctly, it is easy to modify the model to calculate dS/dy and so I can be assured that my method is sound.

dN_{ch}/dy can be computed by integrating Eq. (51) from Ref. [6]:

$$E \frac{d^3N}{dp^3} = \frac{1}{2\pi p_T} \frac{d^2N}{dp_T dy} \quad (57)$$

and one obtains:

$$\frac{dN}{dy} = \int dp_T 2\pi p_T E \frac{d^3N}{dp^3} \quad (58)$$

In Table 2, the dN_{ch}/dy values from Ref. [2] are shown. In Table 3, my own dN_{ch}/dy values are shown. My results do not show a significant disagreement with the results from Ref. [2]. The minor differences are caused by differences in the selection of the fit region. From this, I conclude, that my approach so far works as intended.

Table 2: dN_{ch}/dy values from Ref. [2]

centrality	0-5%	5-10%
π	733 ± 54	606 ± 42
K	109 ± 9	91 ± 7
p	34 ± 3	28 ± 2

Table 3: dN_{ch}/dy my values

centrality	0-5%	5-10%
π	728 ± 56	600 ± 47
K	109 ± 8	91 ± 7
p	34 ± 2	28 ± 2

The results for dS/dy for each particle species and fit function are shown in Table 4. From the variance of these values, I get an additional systematic error to account for the fit model selection. One can see that the values using different fit functions do not show a significant disagreement. This is plausible, since the fit extrapolation only accounts for the fraction of the yield where no data is available.

Table 4: dS/dy results

fit function	Tsallis-Levy	Bose-Einstein	m_T exponential	Boltzmann
π^+	2367 ± 147	2361 ± 156	2342 ± 146	2322 ± 146
K^+	612 ± 40	613 ± 40	612 ± 40	608 ± 40
p	258 ± 19	259 ± 19	258 ± 19	258 ± 19
Λ^0	214 ± 17	215 ± 17	214 ± 18	214 ± 18
Ξ^-	38 ± 2	38 ± 2	38 ± 2	38 ± 2
Ω^-	8 ± 1	8 ± 1	8 ± 1	8 ± 1

To estimate the final-state entropy from the results in Table 4, one has to include the missing particles from our previously built particle list of Pal and Pratt in Table 1. I obtain the following factors:

- π : 3 for π^+, π^-, π^0
- η : same as K
- η' : same as $\frac{1}{2}p$
- K : 4 for K^+, K^-, K^0, \bar{K}^0
- p : 2 for p, \bar{p}
- Λ : 2 for $\Lambda, \bar{\Lambda}$
- Σ : same as Λ with $\frac{N(\Sigma)}{N(\Lambda)}$, 6 for $\Sigma^\pm, \bar{\Sigma}^\pm, \Sigma^0, \bar{\Sigma}^0$
- Ξ : 4 for $\Xi^-, \Xi^0, \bar{\Xi}^+, \bar{\Xi}^0$
- Ω : 2 for $\Omega, \bar{\Omega}$
- n : same as p , 2 for n, \bar{n}

As formerly described, similar to Eq. 51, the Σ are extracted via the thermodynamical model using Eq. (10.63) from Ref. [7], derived in detail in Sec. 3:

$$N = \sum_{k=1}^{\infty} \frac{Tg}{2\pi^2} \frac{(\text{sign})^{k+1}}{k} m^2 \mathcal{K}_2 \left(\frac{km}{T} \right) \quad (59)$$

with degeneracy $g = 2J + 1$, temperature $T = 156$ MeV, particle mass m and Bessel function \mathcal{K}_n of kind n , the sign is + for bosons and – for fermions.

I take the average of the values from the different fit functions and correct for feeddown by modifying the ROOT [9] script provided by Klaus Reygers [8], the script is explained in Sec. 3, by counting the number of primary and secondary final state hadrons for the corresponding particles. The feeddown ratio for a specific particle species A and decay $M \rightarrow A$, with mother particle M , is calculated by:

$$\text{feeddown ratio} = \frac{\text{number of secondary final state A with mother M}}{\text{total number of final state A}} \quad (60)$$

The $\eta, \eta' \rightarrow \pi$ and $\Sigma, \Xi, \Omega \rightarrow \Lambda$ decays are included, other feeddown processes are neglected as in Pal and Pratt's approach, shown in Table 5.

Table 5: feeddown correction

decay	feeddown ratio
$\eta \rightarrow \pi$	1.2%
$\eta' \rightarrow \pi$	2.1%
$\Sigma \rightarrow \Lambda$	16.5%
$\Xi \rightarrow \Lambda$	negligible
$\Omega \rightarrow \Lambda$	negligible

Similar to Pal and Pratt’s results in Table 1, the contributions to my final-state entropy are shown in Table 6.

Table 6: computing the final-state entropy

particle	dS/dy one charge	factor	dS/dy total
π	2272	3	6816
K	611	4	2444
η			611
η'			129
p	258	2	516
n	258	2	516
Λ	179	2	358
Σ	119	6	714
Ξ	38	4	152
Ω	8	2	16
total sum			12272

The uncertainty of the final-state entropy mainly results from the uncertainty of the invariant yields of the different particle species, additional contributions come from the fit extrapolation (rather small because only a fraction of the yield is extrapolated), HBT radii data uncertainty (a relative error of R_{inv} of 0% would lower the relative error of dS/dy by $\approx 1\%$) and fit model variance (almost negligible as one can see in Table 4). As Pal and Pratt have already observed, the uncertainty is limited by the uncertainty of the measurements of the invariant yields.

The final result for the final-state entropy for Pb-Pb collisions at $\sqrt{s_{NN}} = 2.76$ TeV is:

$$\boxed{\frac{dS}{dy} = 12272 \pm 868 \text{ (7\%)}} \quad (61)$$

3 Entropy estimation from Relativistic Hadron Resonance Gas model

The second method to estimate the final-state entropy for Pb-Pb collisions at $\sqrt{s_{NN}} = 2.76$ TeV at the LHC (centrality 0 – 10%) uses the measured charged particle multiplicity $dN_{ch}/d\eta$ from the ALICE Collaboration 1303.0737 [2] in combination with a relativistic hadron resonance gas model. For the corresponding centralities, the values for $dN_{ch}/d\eta$ given in Ref. [2] are:

$$\frac{dN_{ch}}{d\eta}_{0-5\%} = 1601 \pm 60 \quad (62)$$

$$\frac{dN_{ch}}{d\eta}_{5-10\%} = 1294 \pm 49 \quad (63)$$

$$\frac{dN_{ch}}{d\eta}_{0-10\%} = 1448 \pm 54 \quad (64)$$

The value for the centrality 0 – 10% simply consists of the average of these values.

For the conversion of $\frac{dN_{ch}}{d\eta}$ to $\frac{dN_{ch}}{dy}$, the ratio $\frac{dN_{ch}}{dy} / \frac{dN_{ch}}{d\eta}$ is needed. For a given particle species, this can be calculated from the invariant yields using Eq. (44) from Ref. [6] and integrating Eq. (51) from Ref. [6]:

$$\frac{d^2N}{d\eta dp_T} = \sqrt{1 - \frac{m^2}{m_T^2 \cosh^2 y}} \frac{d^2N}{dy dp_T} \quad (65)$$

$$\frac{dN}{dy} = \int dp_T 2\pi p_T E \frac{d^3N}{dp^3} \quad (66)$$

with $m_T = \sqrt{m^2 + p_T^2}$. For $y \approx 0$, the $\cosh y$ term approaches unity and can be neglected. I then get for $dN/d\eta$:

$$\frac{dN}{d\eta} = \int dp_T \sqrt{1 - \frac{m^2}{m_T^2}} 2\pi p_T E \frac{d^3N}{dp^3} \quad (67)$$

To compute the total values, one has to take multiple particle species into account. Here, I include pions, kaons and protons, each of these with a factor 2 because there are two charged states for each species, i.e. π^+ and π^- , K^+ and K^- , and p and \bar{p} . The total $\frac{dN_{ch}}{dy}$ and $\frac{dN_{ch}}{d\eta}$ are then given by:

$$\sum \frac{dN_{ch}}{dy} = 2 \frac{dN_{ch}}{dy}_{\pi} + 2 \frac{dN_{ch}}{dy}_K + 2 \frac{dN_{ch}}{dy}_p \quad (68)$$

$$\sum \frac{dN_{ch}}{d\eta} = 2 \frac{dN_{ch}}{d\eta}_{\pi} + 2 \frac{dN_{ch}}{d\eta}_K + 2 \frac{dN_{ch}}{d\eta}_p \quad (69)$$

and the total ratio by:

$$\frac{\frac{dN_{ch}}{dy}}{\frac{dN_{ch}}{d\eta}} = \frac{\sum \frac{dN_{ch}}{dy}}{\sum \frac{dN_{ch}}{d\eta}} \quad (70)$$

The resulting $\frac{dN_{ch}}{dy} / \frac{dN_{ch}}{d\eta}$ can now be calculated with the invariant yields I used in my first method (π , K , p data from Ref. [2]) with the same approach as described in Ref. [2] for $\frac{dN_{ch}}{dy}$,

which I applied and explained in detail in Sec. 2. The ratio is calculated in many trials using Monte Carlo, while simultaneously computing $\Sigma \frac{dN_{ch}}{dy}$ and $\Sigma \frac{dN_{ch}}{d\eta}$ in the same trial (because they are related by Eq. 65). I get as a result:

$$\frac{\frac{dN_{ch}}{dy}}{\frac{dN_{ch}}{d\eta}} = 1.162 \pm 0.008 \quad (71)$$

To obtain dS/dy , the ratio N/N_{ch} is also needed, which is calculated by a ROOT [9] script by Klaus Reygers [8] and works as follows:

- get all (anti)particles, excl. K_S^0, K_L^0 , with a mass of ≤ 2 GeV with Pythia8 [10]
- assumptions:
 - p_T distribution: $\frac{dn}{dp_T} = A_{\text{norm}} p_T \exp\left(-\sqrt{p_T^2 + m^2}/T\right)$
 - sudden freezeout at $T_{ch} = 0.156$ GeV
 - lifetime after that a particle is considered stable: $\tau_0^{\text{max}} = 10^{-5}$ mm/c
- generate many events with random azimuthal angle ϕ , rapidity y and p_T of the hadron
- loop over primary particles and fill primary histogram
- let particles decay with Pythia8 decayer [10]
- fill histograms with final state primary particles (charged/non-charged)
- loop over decay particles
- fill histograms with final state secondary particles (charged/non-charged)
- integrate histograms and calculate the ratio $N^{\text{primary}}/N_{ch}^{\text{final}}$

The particle lifetime is chosen such that particles included in the list of Pal and Pratt, see Sec. 2, are considered stable. We get the result:

$$\frac{N}{N_{ch}} = 1.16 \quad (72)$$

Note: We crosschecked the result for N/N_{ch} for only π and get the expected 1.5 ratio.

Because the Pythia8 particle list does not include all particles that can be found in the Particle Data Group (2016) [11], I additionally calculate N/N_{ch} from the results of the statistical hadronization model by Andronic, Braun-Munzinger et al. [30]. This model only depends on the temperature, the baryochemical potential and the volume, assumes a rapid chemical freezeout and includes all known hadrons. It uses the same volume correction as the thermal model described in Ref. [23], explained in Sec. 1.3.6. For Pb-Pb collisions at $\sqrt{s_{NN}} = 2.76$ TeV at the LHC with a centrality of 0 – 10%, they obtain for the volume at freezeout $V = 5280$ fm³, see Figure 13. From Ref. [23], Figure 6, I extract the value for the number density n (with volume correction), which allows me to compute the number of primary hadrons N^{primary} :

$$V = 5280 \text{ fm}^3 \quad (73)$$

$$n = \frac{N}{V} = 0.355 \text{ fm}^{-3} \quad (74)$$

$$N^{\text{primary}} = nV = 1874 \quad (75)$$

With Eq. 64 and Eq. 71, I get for dN_{ch}/dy :

$$\frac{dN_{ch}}{dy} = 1683 \pm 4\% \quad (76)$$

$$N_{ch}^{\text{final}} = 1 \frac{dN_{ch}}{dy} = 1683 \quad (77)$$

using a rapidity interval of $|y| < 0.5$. This gives me the ratio $N^{\text{primary}}/N_{ch}^{\text{final}}$:

$$\frac{N}{N_{ch}} = 1.11 \quad (78)$$

For my result, I take the average of Eqs. 72 and 78. For the uncertainty, I use half of the difference between Eqs. 72 and 78. I obtain as result:

$$\frac{N}{N_{ch}} = 1.14 \pm 2\% \quad (79)$$

For the computation of the entropy per hadron, the important choices are the value of the chemical freezeout temperature and the list of included particles. I get the chemical freezeout temperature from the statistical hadronization model by Andronic, Braun-Munzinger et al. [30]. As one can see in Figure 13, the particle yields predicted by the statistical model are in good agreement with the ALICE data. Also, one can compare the chemical freezeout temperature from the statistical model to Lattice QCD calculations done by Ding, Karsch et al. [29], shown in Figure 14. It is apparent that the chemical freezeout temperature of $T = 156.5$ MeV obtained by Andronic, Braun-Munzinger et al. is compatible with the critical temperature of $T = 154 \pm 9$ MeV obtained in the Lattice QCD calculations.

For my computation, I adopt the following value for the chemical freezeout temperature:

$$T_{ch} = 156 \pm 9 \text{ MeV} \quad (80)$$

My particle list consists of all mesons and baryons from the Particle Data Group (2016) [11]. A total of 537 particles are included. The entropy per hadron S/N is then calculated by summing up the entropy densities and number densities of all included particles:

$$\frac{S}{N} = \frac{\sum_{\text{particles}} S}{\sum_{\text{particles}} N} \quad (81)$$

As described in the book *Hadrons and Quark-Gluon Plasma* by Letessier and Rafelski [7] (Sec. 10), for a relativistic gas, the total partition function $\ln \mathcal{Z}$ can be obtained by summing up the logarithms of the different flavors:

$$\ln \mathcal{Z} = \sum_f \ln \mathcal{Z}_f \quad (82)$$

with for each flavor of an ideal Fermi (F) or Bose (B) gas:

$$\ln \mathcal{Z}_{F,B} = \pm g_{F,B} V \int \frac{d^3 p}{(2\pi)^3} [\ln(1 \pm \gamma \lambda e^{-\beta \epsilon}) + \ln(1 \pm \gamma \lambda^{-1} e^{-\beta \epsilon})] \quad (83)$$

with degeneracy $g = 2J + 1$, volume V , upper (lower) sign for fermions (bosons), normalization constant γ , $\lambda = e^{\mu/\beta}$ with chemical potential μ , $\beta = 1/T$ with temperature T and single-particle

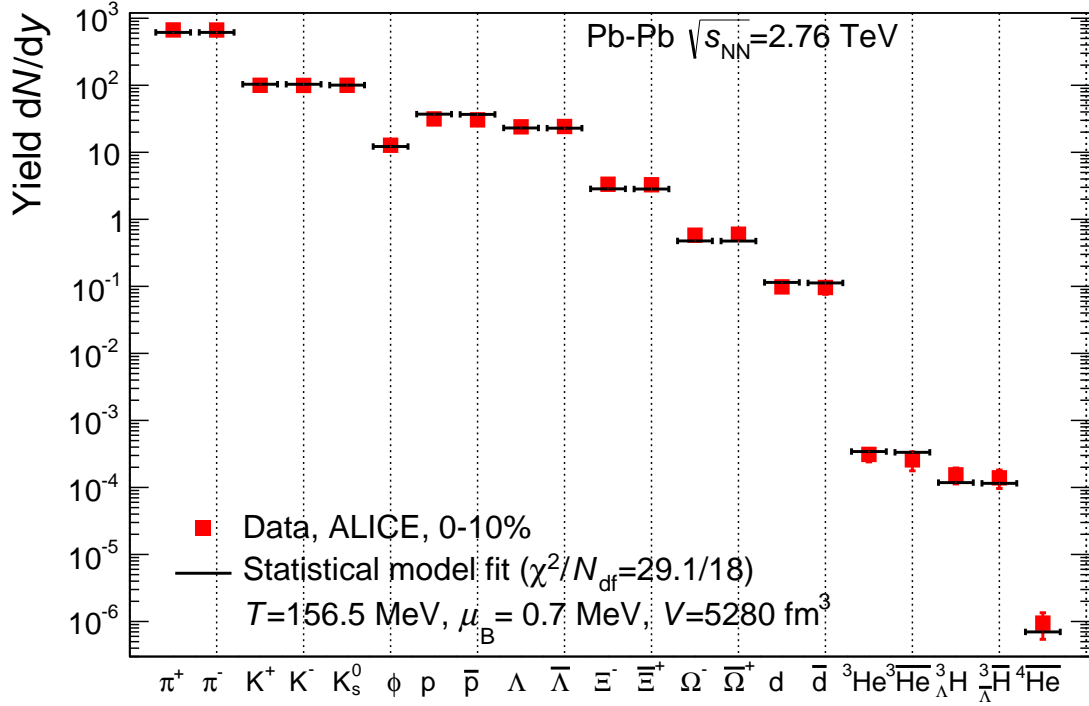


Figure 13: Hadron multiplicities measured in Pb-Pb collisions (0 – 10%) at the LHC in comparison with statistical model fits done by Andronic, Braun-Munzinger et al. [30]

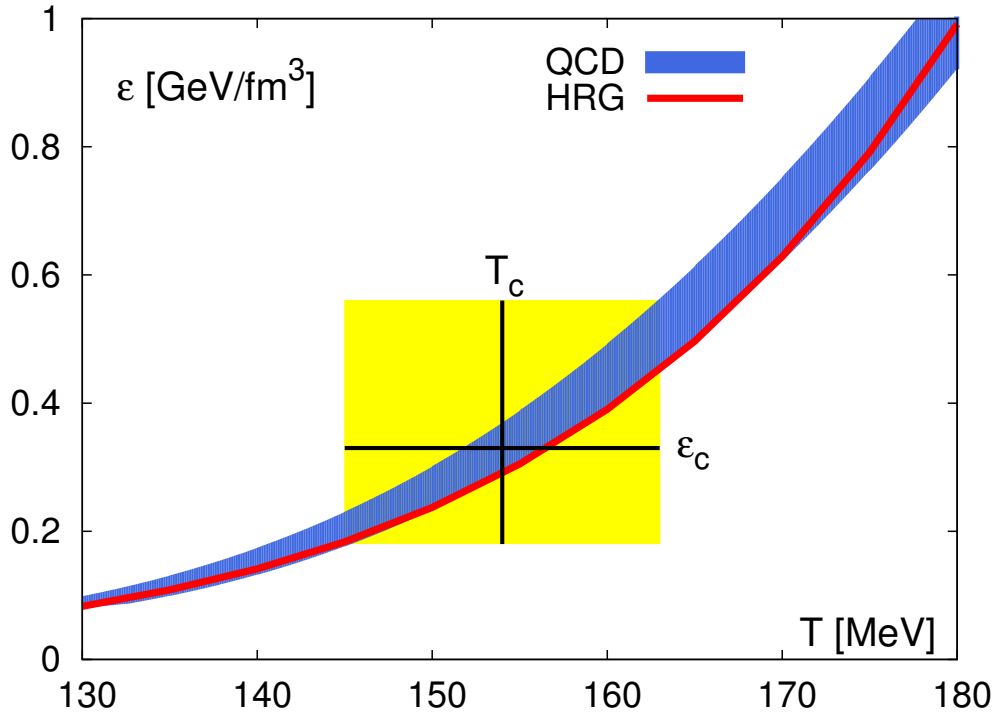


Figure 14: critical energy density and critical temperature in Lattice QCD calculations by Ding, Karsch et al. [29]

energy ϵ . Employing the series expansion, one gets:

$$\ln \mathcal{Z} = \frac{\beta^{-3}V}{2\pi^2} \sum_{n=1}^{\infty} g(\mp)^{n+1} \frac{\lambda^n}{n^3} (n\beta m)^2 \mathcal{K}_2(n\beta m) \quad (84)$$

with particle mass m and Bessel function \mathcal{K}_n of kind n . As explained earlier, I use a temperature of $T = 156 \pm 9$ MeV during my computations. I also neglect the baryochemical potential at LHC energy, i.e. $\mu_B \approx 0$, which results in $\lambda = 1$. The number density n for a given particle species is then given by:

$$n = \frac{N}{V} = \frac{\lambda}{V} \frac{\partial}{\partial \lambda} \ln \mathcal{Z} = \sum_{k=1}^{\infty} \frac{Tg}{2\pi^2} \frac{(\mp)^{k+1}}{k} m^2 \mathcal{K}_2\left(\frac{km}{T}\right) \quad (85)$$

and the entropy per particle by:

$$\frac{S}{N} = \frac{\ln \mathcal{Z} - \beta \frac{\partial}{\partial \beta} \ln \mathcal{Z}}{\lambda \frac{\partial}{\partial \lambda} \ln \mathcal{Z}} - \ln \lambda = 4 \frac{\sum_{k=1}^{\infty} \frac{(\mp)^k}{k^4} \left(\left(\frac{km}{T}\right)^2 \mathcal{K}_2\left(\frac{km}{T}\right) + \frac{1}{4} \left(\frac{km}{T}\right)^3 \mathcal{K}_1\left(\frac{km}{T}\right) \right)}{\sum_{k=1}^{\infty} \frac{(\mp)^k}{k^3} \left(\frac{km}{T}\right)^2 \mathcal{K}_2\left(\frac{km}{T}\right)} \quad (86)$$

Combining these two equations, the entropy density s of a given particle species is:

$$s = \frac{S}{V} = \mp \frac{4gT^3}{2\pi^2} \sum_{k=1}^{\infty} \frac{(\mp)^k}{k^4} \left(\left(\frac{km}{T}\right)^2 \mathcal{K}_2\left(\frac{km}{T}\right) + \frac{1}{4} \left(\frac{km}{T}\right)^3 \mathcal{K}_1\left(\frac{km}{T}\right) \right) \quad (87)$$

I cut off to the sum after the first 20 terms because one cannot sum up to infinity and the contribution of high terms vanishes.

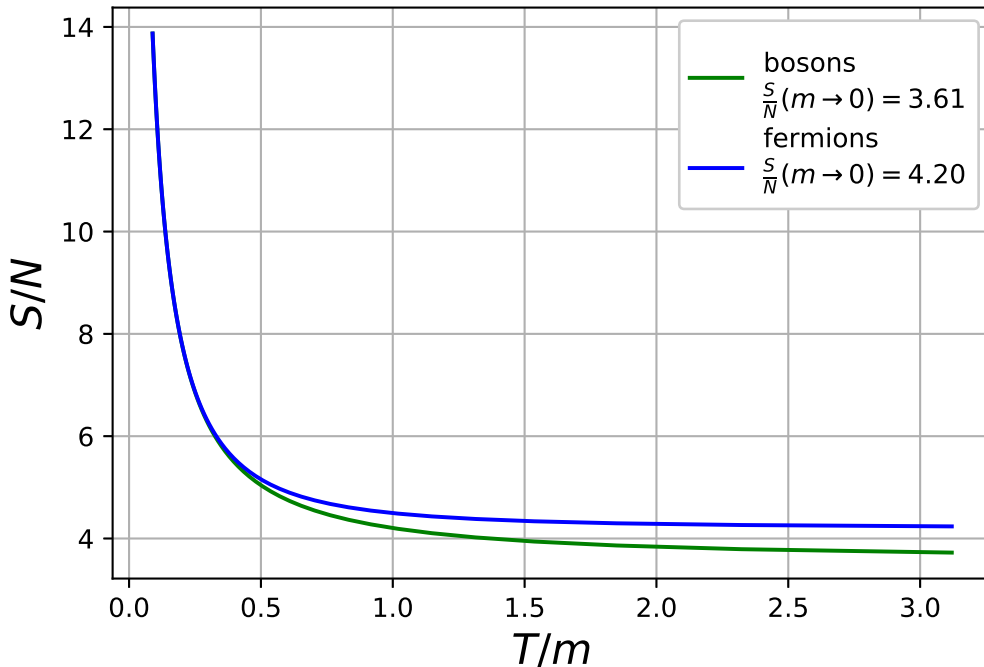


Figure 15: S/N crosscheck

To verify Eq. 85 and Eq. 87, a crosscheck with Ref. [7] is done. I plot S/N over T/m and get the values of the entropy per hadron of bosons and fermions for vanishing particle mass,

i.e. $T/m \rightarrow \infty$, shown in Figure 15. The plot looks as expected. I obtain the same relativistic limits as in Ref. [7]:

$$\frac{S}{N_B}(m \rightarrow 0) = 3.61 \quad (88)$$

$$\frac{S}{N_F}(m \rightarrow 0) = 4.20 \quad (89)$$

with the indices F for fermion and B for boson. To visualize how S/N builds up to its final value, I plot the total S/N value while increasing the number of included particles, starting by the lowest mass (π), shown in Figure 16. As one can see, the final value of the entropy per hadron builds up rather fast, so neglecting the high-mass resonances does not significantly change the result, making it robust to new discoveries of high-mass resonances missing in the particle list.

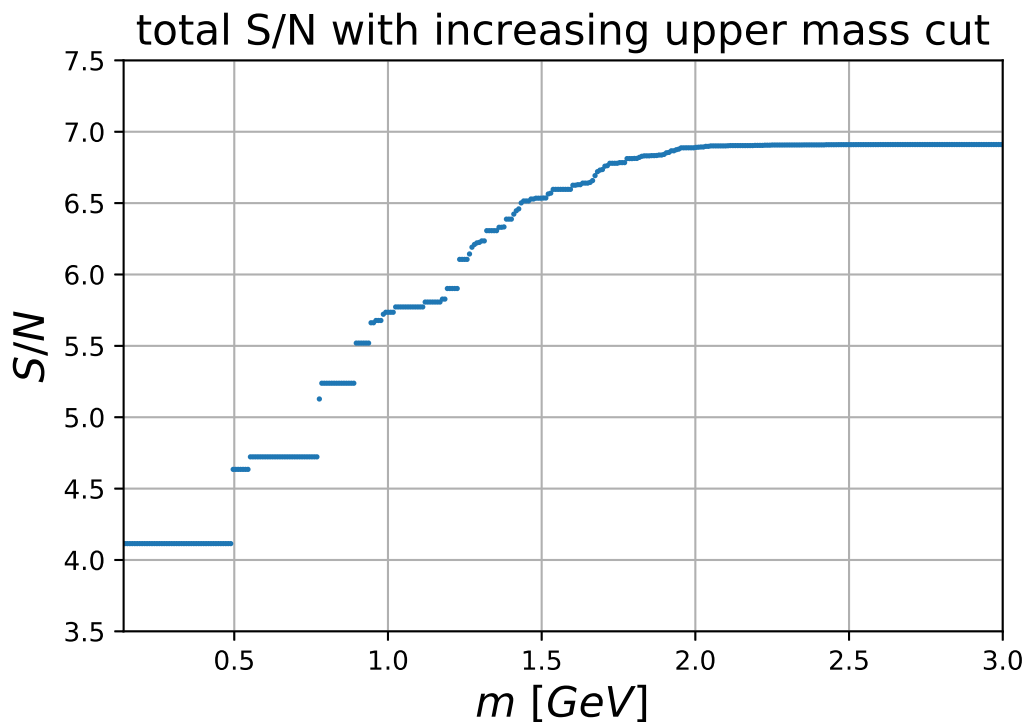


Figure 16: total S/N with increasing upper mass cut

The final value for the entropy per hadron S/N is:

$$\frac{S}{N} = 6.91 \pm 6\% \quad (90)$$

An uncertainty of 3% results from the uncertainty on the chemical freezeout temperature $T_{ch} = 156 \pm 9$ MeV. Neglecting the width of states of the included particles results in an additional uncertainty of 3%, as noted in Ref. [14].

Using Eqs. 64, 71, 79 and 90, the final result for dS/dy can be calculated the following way:

$$\frac{dS}{dy} = \frac{dN_{ch}}{dy} \frac{S}{N_{ch}} = \frac{dN_{ch}}{dy} \frac{N}{N_{ch}} \frac{S}{N} = \frac{\frac{dN_{ch}}{dy}}{\frac{dN_{ch}}{d\eta}} \frac{dN_{ch}}{d\eta} \frac{N}{N_{ch}} \frac{S}{N} \quad (91)$$

The uncertainty on dS/dy mainly results from the uncertainty on the $dN_{ch}/d\eta$ data from ALICE and from the uncertainty on S/N due to the choice of the chemical freezeout temperature and from neglecting the width of states. Additional small contributions are the uncertainty on $\frac{dN_{ch}}{dy} / \frac{dN_{ch}}{d\eta}$ and N/N_{ch} .

The final result for the final-state entropy for Pb-Pb collisions at $\sqrt{s_{NN}} = 2.76$ TeV is:

$$\boxed{\frac{dS}{dy} = 13243 \pm 984 \text{ (7\%)}} \quad (92)$$

4 Summary

4.1 Pal and Pratt method

In my thesis, in the first method, I apply the method that was introduced by Subrata Pal and Scott Pratt in their paper *Entropy Production at RHIC* [1] for RHIC to Pb-Pb collisions at $\sqrt{s_{NN}} = 2.76$ TeV at the LHC, explained in detail in Sec. 2. I get as a result for the final-state entropy:

$$\boxed{\frac{dS}{dy} = 12272 \pm 868 \text{ (7\%)}} \quad (93)$$

Using the value for the charged particle multiplicity from Ref. [2]:

$$\frac{dN_{ch}}{d\eta} = 1448 \pm 4\% \quad (94)$$

(centrality 0 – 10%) and a conversion factor of $\frac{dN_{ch}}{dy} / \frac{dN_{ch}}{d\eta} = 1.162$ (from my calculations explained in Sec. 3) results in $dN_{ch}/dy = 1683 \pm 4\%$. I estimate for the entropy per charged hadron:

$$\frac{S}{N_{ch}} = \frac{dS/dy}{dN_{ch}/dy} = 7.29 \pm 7\% \quad (95)$$

My result for the entropy per charged hadron agrees well with the result of Pal and Pratt of $S/N_{ch} = 7.2 \pm 10\%$. This is not surprising as I closely followed Pal and Pratt's recipe and the entropy per hadron is expected to be a robust freezeout criterion over a wide $\sqrt{s_{NN}}$ range, as noted in Ref. [21].

4.2 Relativistic Hadron Resonance Gas model

In my second method, explained in Sec. 3, I estimate the entropy from the charged particle multiplicity using a relativistic hadron gas model as described in Ref. [7]. In this model, the entropy per hadron is a directly calculated thermodynamic quantity:

$$\frac{S}{N} = 6.91 \pm 6\% \quad (96)$$

The uncertainty results from the uncertainty on the chemical freezeout temperature $T_{ch} = 156 \pm 9$ MeV and from neglecting the width of states. I note that my result for S/N is identical with the calculations done by Müller and Rajagopal in Ref. [14] for the same choice of the chemical freezeout temperature, i.e. I also obtain $S/N = 7.25$ at a temperature of $T_{ch} = 170$ MeV. I used a different chemical freezeout temperature than Müller and Rajagopal because of the recent results of the statistical hadronization model by Andronic, Braun-Munzinger et al. [30]. Using N/N_{ch} from Eq. 79 gives an entropy per charged hadron of:

$$\frac{S}{N_{ch}} = 7.87 \pm 6\% \quad (97)$$

With $dN_{ch}/dy = 1683 \pm 4\%$, the entropy rapidity density can be computed by:

$$\frac{dS}{dy} = \frac{S}{N_{ch}} \frac{dN_{ch}}{dy} \quad (98)$$

The result for the final-state entropy for Pb-Pb collisions at $\sqrt{s_{NN}} = 2.76$ TeV at the LHC is:

$$\boxed{\frac{dS}{dy} = 13243 \pm 984 \text{ (7\%)}} \quad (99)$$

My result for the final-state entropy obtained by this method is in good agreement with the result of the first method $dS/dy = 12272 \pm 868$ (7%).

4.3 Overview and Synthesis of methods for entropy estimation

For an easy comparison, I now give an overview of the results of all methods presented in Sec. 1 and the results of my thesis in Table 7:

Table 7: Results of all presented methods for entropy estimation

Method	S/N_{ch}	S/N	N/N_{ch}	comment
Bjorken flow (Ch. 1.3.1)	≈ 5			rough approximation
phase space density (Ch. 1.3.2)	7.7	5.15	1.5	$T_{ch} = 170$ MeV
Pal and Pratt (Ch. 1.3.2)	$7.2 \pm 10\%$			
immed. equilibration (Ch. 1.3.3)	7.5			
hadron resonance gas (Ch. 1.3.4)	$6.97 \pm 6\%$	$7.25 \pm 6\%$	1/1.04	$T_{ch} = 170 \pm 10$ MeV
thermal model (Ch. 1.3.5)		$7.16 \pm 8\%$		
interact. hadron gas (Ch. 1.3.6)		7.28		without volume corr.
interact. hadron gas (Ch. 1.3.6)		7.61		with volume corr.
this work (Pal, Pratt) (Ch. 2)	$7.29 \pm 7\%$			
this work (HRG) (Ch. 3)	$7.87 \pm 6\%$	$6.91 \pm 6\%$	$1.14 \pm 2\%$	$T_{ch} = 156 \pm 9$ MeV

For the entropy per charged hadron S/N_{ch} , except for the Bjorken flow method which is only a rough approximation, there is no major disagreement between the different methods. For the entropy per hadron S/N , the value of the phase space method is significantly lower than the values extracted from the other methods, but as the authors note, that simplified model only provides an approximation. While the hadron resonance gas model used in this work is identical to the hadron resonance gas model presented in Sec. 1.3.4, I used a lower value for the chemical freezeout temperature, $T_{ch} = 156 \pm 9$ MeV instead of $T_{ch} = 170 \pm 10$ MeV, resulting in a lower value for the entropy per hadron. The interacting hadron gas model and the thermal model are both in agreement with the values from the hadron resonance gas model. There are several important choices to be made in theoretical models:

- list of included particles: not including resonances like Δ lowers the entropy per hadron while neglecting high-mass resonances ($m > 2$ GeV) does not significantly change its value
- chemical freezeout temperature T_{ch} : extracted from statistical models, older computations generally use higher values than newer ones, often $T_{ch} = 170$ MeV, which increases the entropy per hadron
- number of hadrons per charged hadron N/N_{ch} : particles decays have significant influence on its value and have to be included, the π value 1.5 is sometimes used instead of a detailed calculation

- level of detail: interactions, width of states, etc. should be considered in the model or if possible included in systematic uncertainties

With this in mind, the advantage of data-driven methods like that of Pal and Pratt becomes apparent, there are fewer theoretical assumptions to be made. Instead, the uncertainties on the measurements, mainly that on the invariant yield, are the limiting factor and there is significant progress being made to reduce them. With the excellent agreement between the result of Pal and Pratt for RHIC, $S/N = 7.2 \pm 10\%$, and my result for LHC with the same method, $S/N = 7.29 \pm 7\%$, one can hope to further refine this value using newer experimental data.

4.4 Interpretation

To interpret my findings, I compute the initial temperature T_0 at the time $\tau_0 = 1 \text{ fm}/c$. This can be done by using the relation of the entropy density s to the temperature T from Ref. [14]:

$$s = \frac{2\pi^2}{45} \nu(T) T^3 \quad (100)$$

with the effective number of thermodynamic degrees of freedom $\nu(T)$, which is temperature-dependent. For an ideal gas of gluons and three flavors of quarks, one gets the non-interaction limit $\nu_{\text{non-int.}} = 47.5$. Lattice QCD calculations [29] show that $\nu(T)$ increases sharply below $\approx 1.5 T_c$ and then converges to a value of about $\nu(T) = 0.8 \nu_{\text{non-int.}}$, shown in Figure 17.

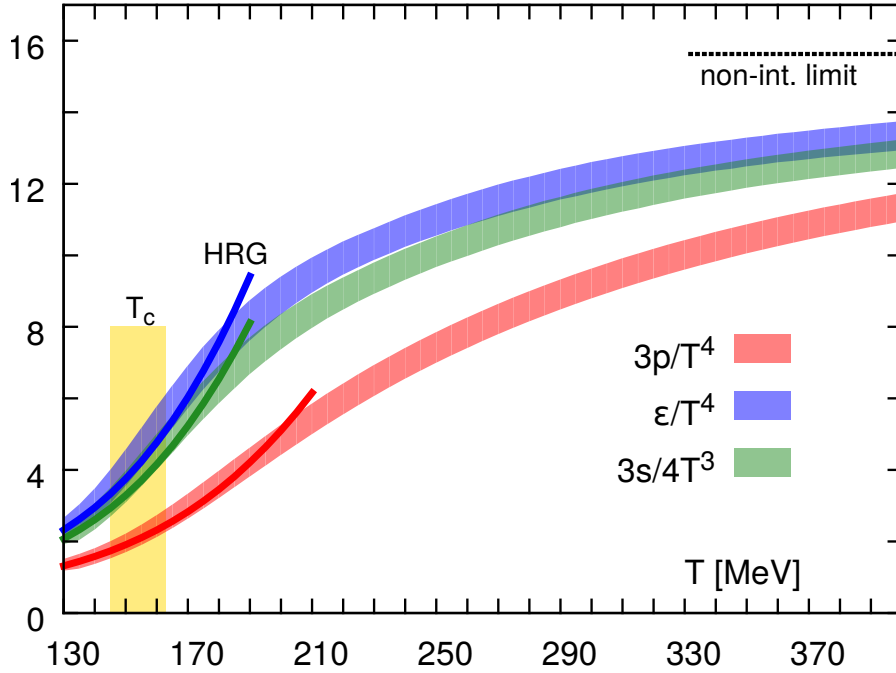


Figure 17: pressure, energy density and entropy density from Lattice QCD calculations compared to a hadron resonance gas and non-interaction limit [29]

To calculate the initial temperature T_0 , I need to compute the entropy density s at the time $\tau_0 = 1 \text{ fm}/c$. The entropy density s is given by the Bjorken relation [15]:

$$s = \frac{S}{V} = \frac{1}{A\tau_0} \left. \frac{dS}{dy} \right|_{y=0} \quad (101)$$

(as described in Sec. 1.3.1) with the entropy S and the volume V :

$$S = 1 \frac{dS}{dy} = 12272 \quad (102)$$

$$V = A\tau_0 = \pi R_{\text{Pb}}^2 \tau_0 = \pi (6.62 \text{ fm})^2 1 \text{ fm} = 138 \text{ fm}^3 \quad (103)$$

The entropy is calculated with the result of Sec. 2 and a rapidity interval of $|y| < 0.5$. The volume is calculated with a lead radius of $R_{\text{Pb}} = 6.62 \text{ fm}$. I get an entropy density of:

$$s = 89.1 \text{ fm}^{-3} \quad (104)$$

$$s = 0.681 \text{ GeV}^3 \quad (105)$$

where I used the relation $\hbar c = 1 = 0.197 \text{ GeV fm}$. With the result for the entropy density and Figure 17, I estimate for the initial temperature T_0 :

$$\boxed{T_0 = 349 \text{ MeV} = 2.24 T_c} \quad (106)$$

The value of ν at this temperature is $\nu \approx 36.5$.

As one can see, the initial temperature T_0 is well above the critical temperature T_c where the QGP phase is entered. From this I conclude that in Pb-Pb collisions at $\sqrt{s_{NN}} = 2.76 \text{ TeV}$ at the LHC, the QGP is produced.

List of Figures

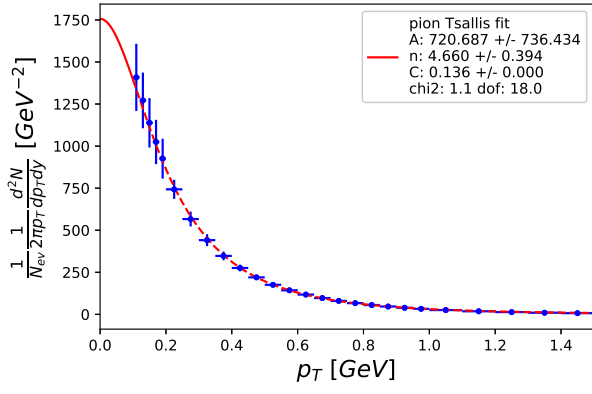
1	QCD phase diagram in temperature and baryochemical potential [29]	5
2	Events recorded by ALICE from the first lead ion collisions in 2011 [34]	6
3	ALICE detector setup [33]	7
4	central collision compared to peripheral collision [33]	8
5	relativistic heavy-ion collision [35]	8
6	space time evolution of a relativistic heavy-ion collision [31]	9
7	ultra-relativistic lead-lead collision (micro-bang) and big bang [7]	10
8	orientation of the out-side-long axes for a viewer perpendicular (left) and parallel (right) to the beam axis [26]	16
9	result of Pal and Pratt [1]	18
10	R_{inv} fits	19
11	π fits	20
12	selected K , p , Λ , Ξ , Ω fits	21
13	Hadron multiplicities measured in Pb-Pb collisions (0 – 10%) at the LHC in comparison with statistical model fits done by Andronic, Braun-Munzinger et al. [30]	28
14	critical energy density and critical temperature in Lattice QCD calculations by Ding, Karsch et al. [29]	28
15	S/N crosscheck	29
16	total S/N with increasing upper mass cut	30
17	pressure, energy density and entropy density from Lattice QCD calculations compared to a hadron resonance gas and non-interaction limit [29]	34
18	π fits	40
19	K fits	41
20	p fits	42
21	Λ fits	43
22	Ξ fits	44
23	Ω fits	45

References

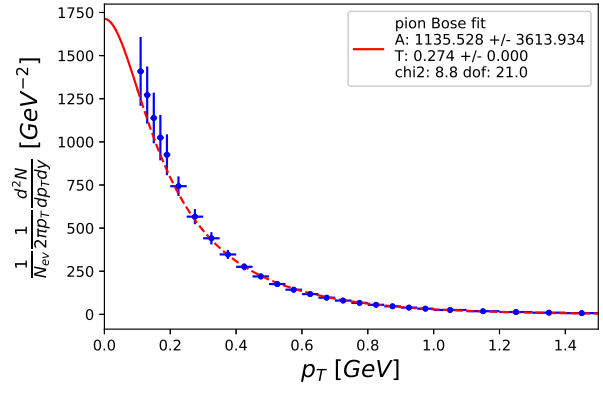
- [1] Pal, Subrata, and Scott Pratt. "Entropy production at RHIC." *Physics Letters B* 578.3-4 (2004): 310-317., URL: <https://arxiv.org/abs/nucl-th/0308077>
- [2] ALICE Collaboration. "Centrality dependence of π , K, p production in Pb-Pb collisions at $\sqrt{s_{NN}}= 2.76$ TeV." arXiv preprint arXiv:1303.0737 (2013)., URL: <https://arxiv.org/abs/1303.0737>
- [3] ALICE Collaboration. "Multi-strange baryon production at mid-rapidity in Pb-Pb collisions at $\sqrt{s_{NN}}= 2.76$ TeV." arXiv preprint arXiv:1307.5543 (2013)., URL: <https://arxiv.org/abs/1307.5543>
- [4] ALICE Collaboration. " K_S^0 and Λ production in Pb-Pb collisions at $\sqrt{s_{NN}}= 2.76$ TeV." arXiv preprint arXiv:1307.5530 (2013)., URL: <https://arxiv.org/abs/1307.5530>
- [5] ALICE Collaboration. "One-dimensional pion, kaon, and proton femtoscopy in Pb-Pb collisions at $\sqrt{s_{NN}}= 2.76$ TeV." arXiv preprint arXiv:1506.07884 (2015)., URL: <https://arxiv.org/abs/1506.07884>
- [6] Sarkar, Sourav, Helmut Satz, and Bikash Sinha, eds. *The physics of the quark-gluon plasma: introductory lectures*. Vol. 785. Springer, 2009.
- [7] Letessier, Jean, and Johann Rafelski. *Hadrons and quark-gluon plasma*. Vol. 18. Cambridge University Press, 2002.
- [8] Klaus Reygers, Physikalisches Institut, Im Neuenheimer Feld 226, 69120 Heidelberg, Germany
- [9] CERN, ROOT. "A Data Analysis Framework." (2014)., URL: <https://root.cern.ch/>
- [10] T. Sjöstrand, S. Mrenna and P. Skands, *JHEP*05 (2006) 026, *Comput. Phys. Comm.* 178 (2008) 852. , URL: <http://home.thep.lu.se/~torbjorn/Pythia.html>
- [11] C. Patrignani et al. (Particle Data Group), *Chin. Phys. C*, 40, 100001 (2016), URL: <http://pdg.lbl.gov/>
- [12] Berges, Jurgen, et al. "What shines brighter, Glasma or quark-gluon Plasma: a parametric estimate of photon production at early times in heavy-ion collisions." arXiv preprint arXiv:1701.05064 (2017)., URL: <https://arxiv.org/abs/1701.05064v2>
- [13] Gubser, Steven S., Silviu S. Pufu, and Amos Yarom. "Entropy production in collisions of gravitational shock waves and of heavy ions." *Physical Review D* 78.6 (2008): 066014., URL: <https://arxiv.org/abs/0805.1551>
- [14] Müller, Berndt, and Krishna Rajagopal. "From entropy and jet quenching to deconfinement?." *The European Physical Journal C-Particles and Fields* 43.1-4 (2005): 15-21., URL: <https://arxiv.org/abs/hep-ph/0502174>
- [15] J.D. Bjorken, *Phys.Rev. D*27 (1983) 140-151
- [16] Back, B. B., et al. "The PHOBOS perspective on discoveries at RHIC." *Nuclear Physics A* 757.1-2 (2005): 28-101., URL: <http://xxx.lanl.gov/abs/nucl-ex/0410022>

- [17] Back, B. B., et al. "Significance of the fragmentation region in ultrarelativistic heavy-ion collisions." *Physical Review Letters* 91.5 (2003): 052303., URL: <http://xxx.lanl.gov/abs/nucl-ex/0210015>
- [18] Landau, L. D. "On the multiparticle production in high-energy collisions." *Izv. Akad. Nauk Ser. Fiz.* 17 (1953): 51-64.
- [19] Adcox, K., et al. "Formation of dense partonic matter in relativistic nucleus–nucleus collisions at RHIC: experimental evaluation by the PHENIX collaboration." *Nuclear Physics A* 757.1-2 (2005): 184-283., URL: <http://xxx.lanl.gov/abs/nucl-ex/0410003>
- [20] Nonaka, C. "C. Nonaka, B. Muller, SA Bass, and M. Asakawa, *Phys. Rev. C* 71, 051901 (R)(2005)." *Phys. Rev. C* 71 (2005): 051901., URL: <http://arxiv.org/abs/nucl-th/0501028v1>
- [21] Oliinychenko, D. R., K. A. Bugaev, and A. S. Sorin. "Investigation of hadron multiplicities and hadron yield ratios in heavy ion collisions." arXiv preprint arXiv:1204.0103 (2012)., URL: <https://arxiv.org/abs/1204.0103>
- [22] Andronic, A., P. Braun-Munzinger, and J. Stachel. "Hadron production in central nucleus–nucleus collisions at chemical freeze-out." *Nuclear Physics A* 772.3-4 (2006): 167-199., URL: <https://arxiv.org/abs/nucl-th/0511071>
- [23] Andronic, A., et al. "Interacting hadron resonance gas meets lattice QCD." *Physics Letters B* 718.1 (2012): 80-85., URL: <https://arxiv.org/abs/1201.0693>
- [24] Adam, Jaroslav, et al. "Centrality Dependence of the Charged-Particle Multiplicity Density at Midrapidity in Pb-Pb Collisions at $\sqrt{s_{NN}} = 5.02$ TeV." *Physical review letters* 116.22 (2016): 222302., URL: <https://arxiv.org/abs/1512.06104>
- [25] Brown, R. Hanbury, and R. Q. Twiss. "A test of a new type of stellar interferometer on Sirius." *Nature* 178.4541 (1956): 1046-1048.
- [26] Lisa, Michael Annan, et al. "Femtoscopy in relativistic heavy ion collisions: two decades of progress." *Annu. Rev. Nucl. Part. Sci.* 55 (2005): 357-402. URL: <https://arxiv.org/abs/nucl-ex/0505014>
- [27] Klaus Reygers, Quark-Gluon Plasma Physics summer semester 2017, URL: https://www.physi.uni-heidelberg.de/~reygers/lectures/2017/qgp/qgp_lecture_ss2017.html
- [28] Bertsch, G., M. Gong, and M. Tohyama. "Pion interferometry in ultrarelativistic heavy-ion collisions." *Physical Review C* 37.5 (1988): 1896.
- [29] Ding, Heng-Tong, Frithjof Karsch, and Swagato Mukherjee. "Thermodynamics of strong-interaction matter from Lattice QCD." *Quark–Gluon Plasma* 5. 2016. 1-65., URL: <https://arxiv.org/abs/1504.05274>
- [30] Andronic, A., et al. "Hadron yields, the chemical freeze-out and the QCD phase diagram." *Journal of Physics: Conference Series*. Vol. 779. No. 1. IOP Publishing, 2017., URL: <https://arxiv.org/abs/1611.01347>
- [31] Stock, Reinhard. "7 Relativistic Nucleus-Nucleus Collisions and the QCD Matter Phase Diagram." *Theory and Experiments*. Springer, Berlin, Heidelberg, 2008. 225-315., URL: <https://arxiv.org/abs/0807.1610>

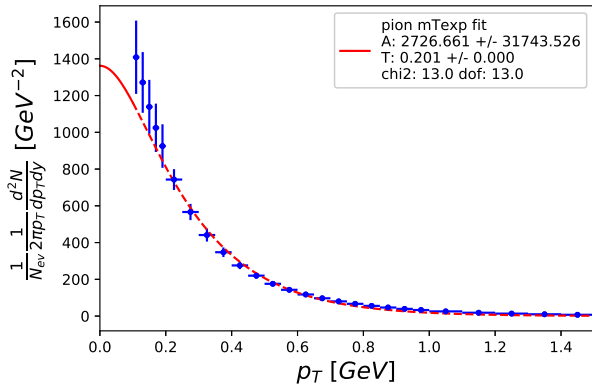
- [32] CERN, European Organization for Nuclear Research, URL: <https://home.cern/>
- [33] Yan, Y., et al. "ALICE A Large Ion Collider Experiment." (1997)., URL: <http://cds.cern.ch/record/5685>
- [34] CERN, CERN-EX-1111290-04, Photograph: Team ALICE, Date: 21 Nov 2011, URL: <https://cdsweb.cern.ch/record/1400435>
- [35] Brookhaven National Laboratory, Relativistic Heavy Ion Collider, URL: <https://www.bnl.gov/RHIC/>
- [36] Aamodt, Kenneth, et al. "The ALICE experiment at the CERN LHC." Journal of Instrumentation 3.08 (2008): S08002., URL: <http://iopscience.iop.org/article/10.1088/1748-0221/3/08/S08002/meta>



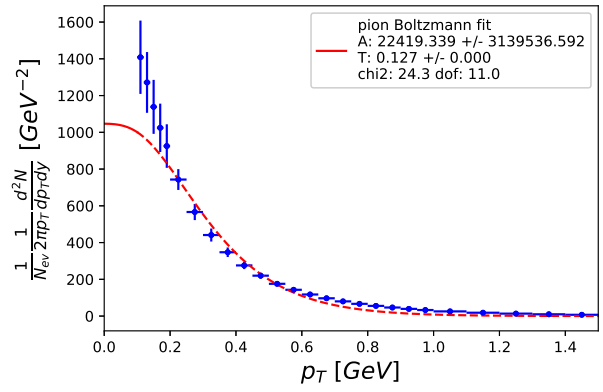
(a) π Tsallis fit



(b) π Bose fit

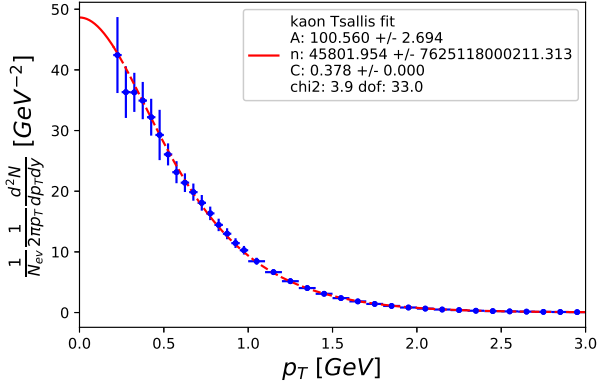


(c) π m_T exp fit

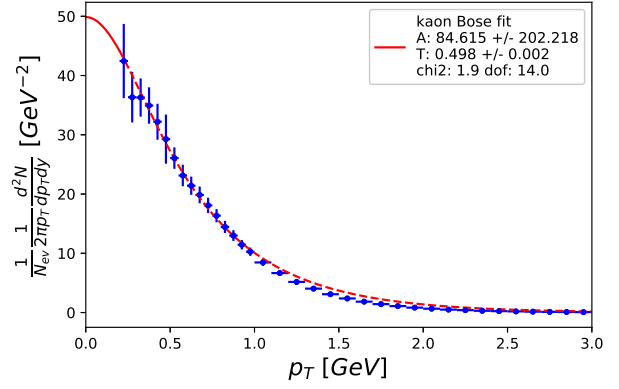


(d) π Boltzmann fit

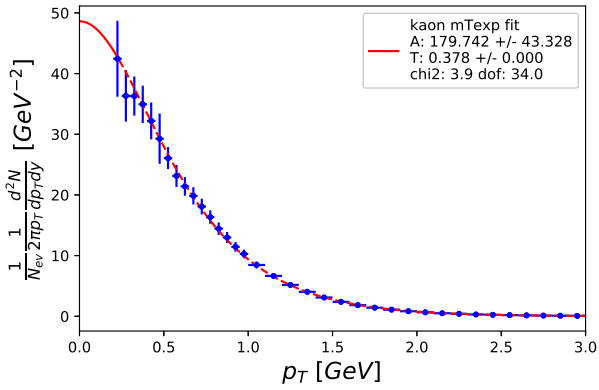
Figure 18: π fits



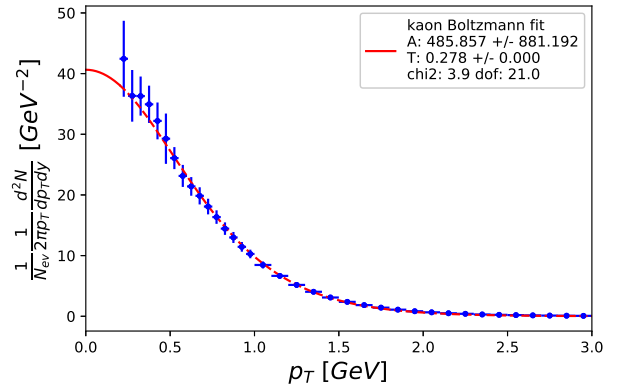
(a) *K* Tsallis fit



(b) *K* Bose fit

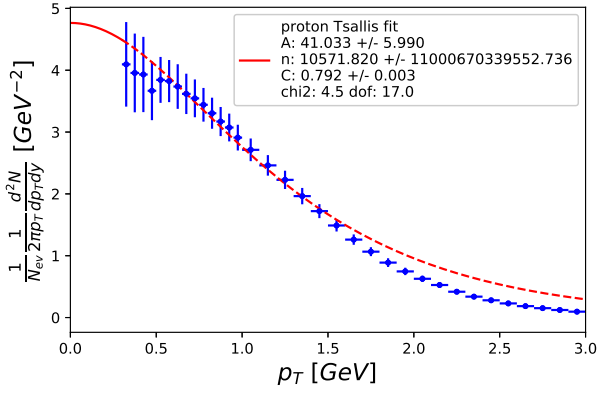


(c) *K* m_T exp fit

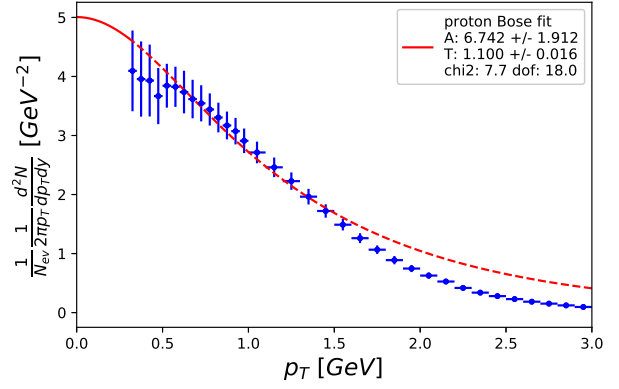


(d) *K* Boltzmann fit

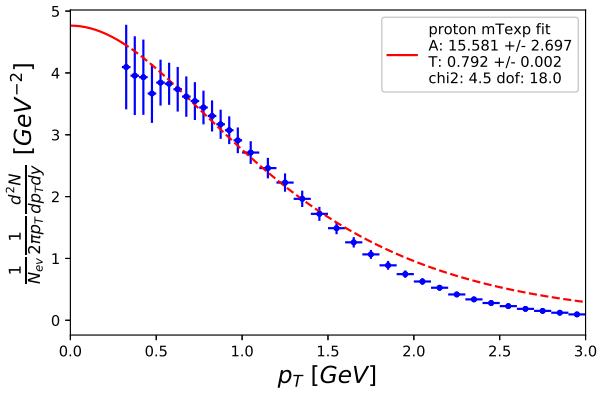
Figure 19: *K* fits



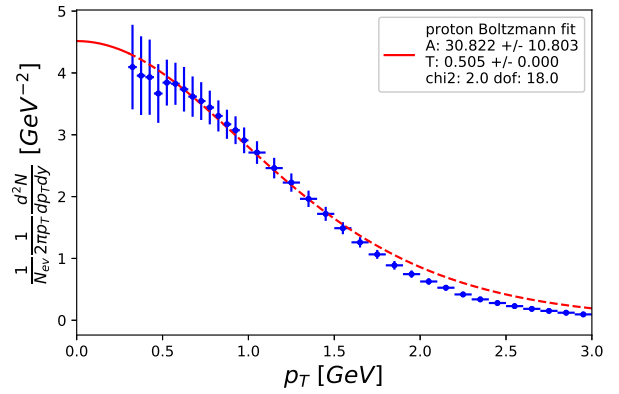
(a) p Tsallis fit



(b) p Bose fit

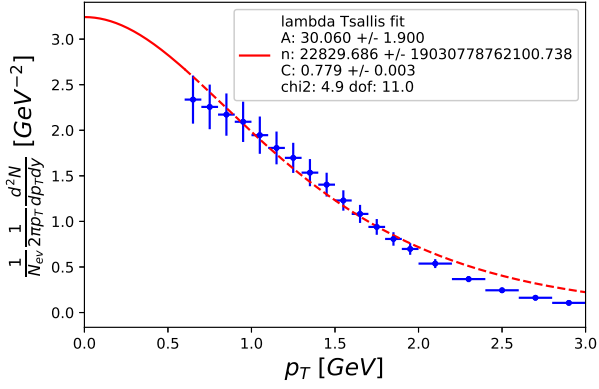


(c) p m_T exp fit

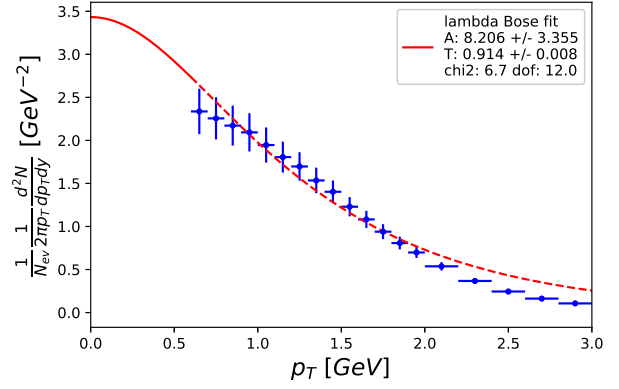


(d) p Boltzmann fit

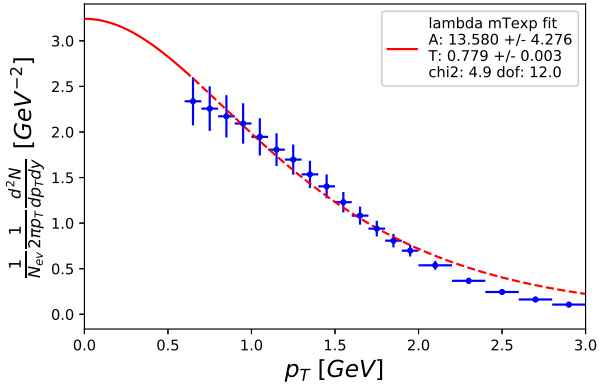
Figure 20: p fits



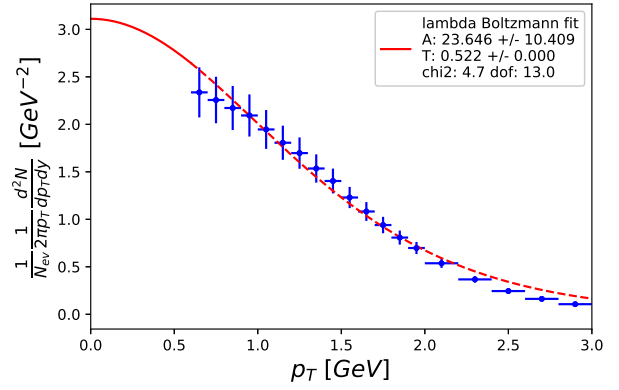
(a) Λ Tsallis fit



(b) Λ Bose fit

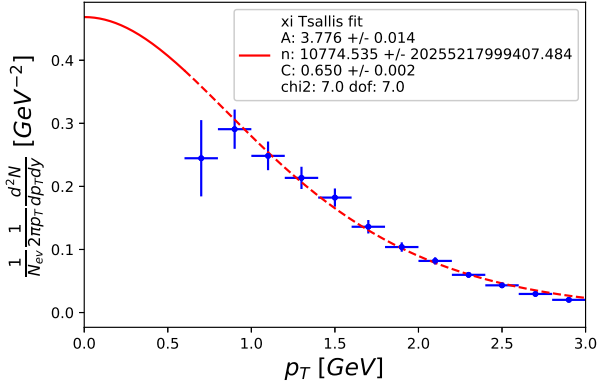


(c) Λ m_T exp fit

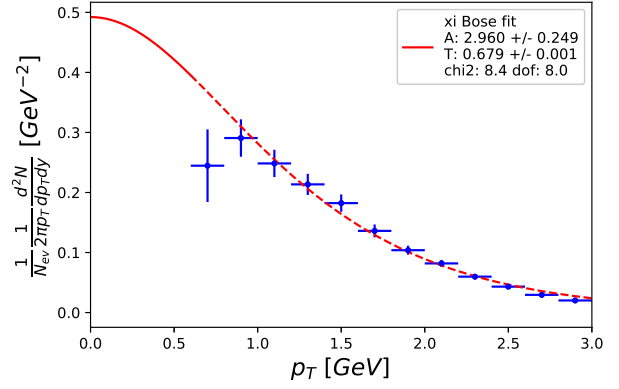


(d) Λ Boltzmann fit

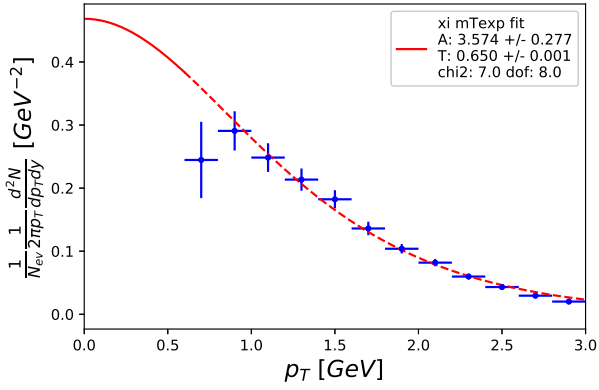
Figure 21: Λ fits



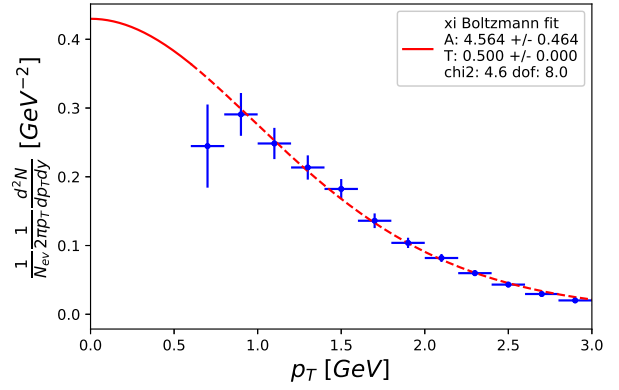
(a) Ξ Tsallis fit



(b) Ξ Bose fit

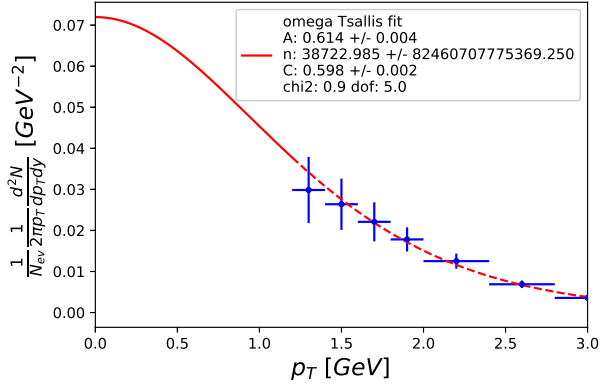


(c) Ξ m_T exp fit

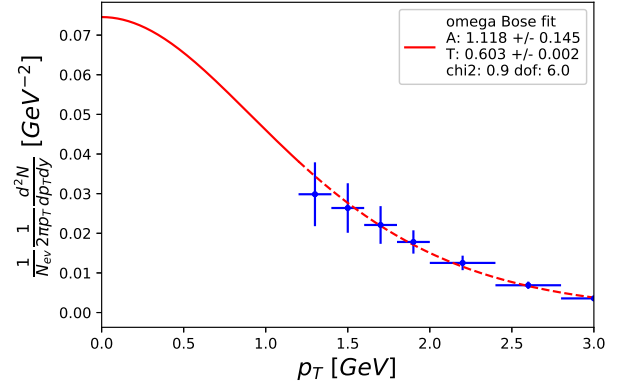


(d) Ξ Boltzmann fit

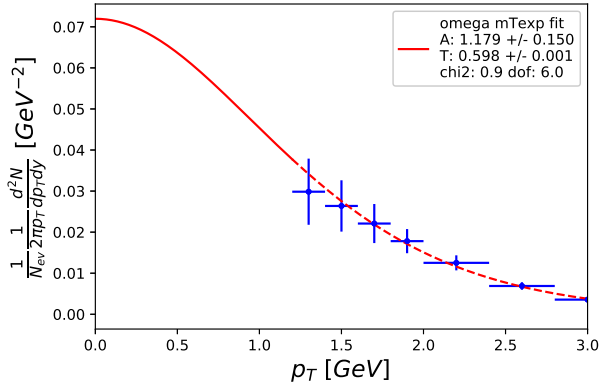
Figure 22: Ξ fits



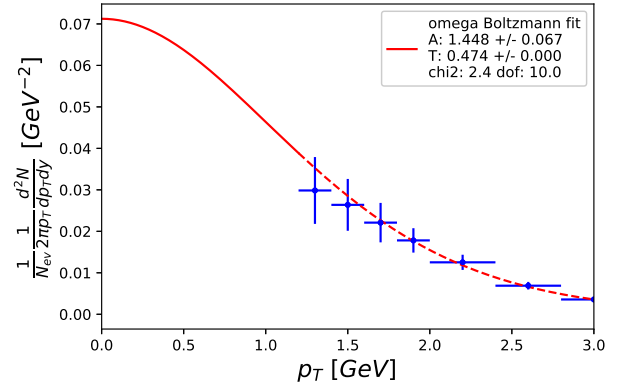
(a) Ω Tsallis fit



(b) Ω Bose fit



(c) Ω m_T exp fit



(d) Ω Boltzmann fit

Figure 23: Ω fits

Erklärung

Ich versichere, dass ich diese Arbeit selbstständig verfasst und keine anderen als die angegebenen Quellen und Hilfsmittel benutzt habe.

Heidelberg, den